UiT The Arctic University of Norway

Faculty of Health Sciences, Department of Pharmacy

Drug Transport and Delivery Research Group

Development of DNA Nanoparticles with Properties for Enhanced Biofilm Uptake

Vegard Borøy

Master's thesis in Pharmacy, May 2022

Supervisors: Dr. Sybil Obuobi, Alexandra Sousa and Professor Nataša Škalko-Basnet

ACKNOWLEDGEMENT

The research presented in this thesis was carried out at the Drug Transport and Delivery Group, Department of Pharmacy at the University of Tromsø (UiT) – The Arctic University of Norway from September 2021 to May 2022.

I would like to start by expressing my sincere gratitude to my main supervisor Dr. Sybil Obuobi for the patient guidance, encouragement, advice, and knowledge you have shared with me. I have been extremely lucky to have a supervisor who cared so much about my work and responded to my questions and queries so promptly. Secondly, I would like to express my gratitude to my co-supervisors PhD student Alexandra Sousa and Professor Nataša Škalko-Basnet for the much valuable feedback throughout this project. I would also like to extend a thanks to the whole Drug Transport and Delivery Research Group for making me feel welcome in the lab.

Finally, I must express my gratitude to my family, friends and fellow pharmacy students for providing continuous encouragement throughout my years of study and the process of researching and writing this thesis. Thank you.

ABSTRACT

Microbial biofilms account for up to 80% of all bacterial infections. They are described as small structural communities of bacteria which are embedded in a self-produced extracellular (EPS) matrix. This EPS matrix poses a substantial challenge for antimicrobial treatment by hindering traversal of antimicrobial agents. Nanotechnology based drug delivery systems (DDS) offer a promising solution to the low antimicrobial efficacy of free drug molecules via encapsulation into optimized carriers to enhance penetration. DNA nanotechnology has drawn considerable interest given the high biocompatibility, excellent structural control and ease of carrier modification, but have properties associated with low biofilm penetration. As such, this project seeks to develop DNA nanoparticles with properties for enhanced biofilm penetration.

A series of DNA nanoparticles were prepared solely via thermal annealing processes or a combination of thermal annealing and polymer coating to achieve four unique carriers with different properties. Characterization of the nanoparticles was performed via dynamic light scattering (DLS). Biofilm penetration of the nanoparticles was evaluated using an in-house dsDNA quantification method, confocal microscopy (CLSM) and fluorescent spectroscopy. Biofilm penetration, biofilm inhibition and effect of the optimized formulation on mature biofilms was tested using crystal violet staining and isothermal microcalorimetry (ICM). The toxicity of the nanoparticles was evaluated against HaCaT cells.

The two modified nanoparticles NMC and NNP^{Chi} had an average size of 22.3 ± 1.3 nm and 297,0 ± 2,9 nm and exhibited a zeta potential of -24.2 ± 3.2 mV and +30.9 ± 1.0 mV respectively. Both nanoparticles showed high biofilm penetration when compared to the control formulation (52.5 ± 10.4 nm and -21.5 ± 3.5 mV). From these, the micellar formulation NMC was chosen for drug loading with polymyxin B (PMB) due to its ideal morphology, small size and affinity to DNA. The optimized PMB loaded formulation significantly inhibited *P. aeruginosa* biofilm growth after co-incubation for 16h and had a significant effect on the time to peak (+444 ± 50 minutes) and relative metabolic rate (20 ± 5%) of mature biofilms after 2h. Toxicity studies on all formulations revealed negligible toxicity.

In conclusion, cationic surface modification and conjugation of a hydrophobic moiety significantly increased the biofilm penetration of DNA nanoparticles. The optimized drug loaded formulation demonstrated promising efficacy against P. *aeruginosa* biofilms.

Keywords: DNA nanotechnology; drug delivery systems; biofilm penetration; polymyxin B

SAMMENDRAG

Bakterier kan danne membrane på sårflater og drastisk hindre heleprosessen. Disse membranene, biofilmer, er implisert i opp mot 80% av alle bakterielle infeksjoner, og beskrives som små strukturelle samfunn av bakterier som er innkapslet i en egenprodusert ekstracellulær polymerisk matrix (EPS). Matriksen utgjør en betydelig utfordring for konvensjonell antimikrobiell behandling ved å hindre deres tilgang til bakteriene. Nanoteknologibaserte drug delivery systemer (DDS) er en utpekt løsning som kan ved å enkapsulere fritt legemiddel i optimaliserte partikler forbedrer evnen til å gjennomtrenge biofilmen. DNA nanoteknologi har fått mye oppmerksomhet på bakgrunn av lav toksisitet og utmerket strukturell kontroll, men DNA har fysiokjemiske egenskaper som generelt er knyttet til dårlig biofilm gjennomtregning. Dette prosjektet ønsket derfor å utvikle en DNA nanopartikkel med optimalisert biofilm-gjennomtregning

En serie DNA nanopartikler ble fabrikkert via hybridisering alene eller hybridisering i kombinasjon med overflatemodifikasjon for å oppnå fire nanopartikler med forskjellig fysiokjemiske egenskaper. Karakterisering av partiklene ble utført via dynamisk lysspredning (DLS). In vitro biofilm gjennomtrenging av partiklene ble evaluert via DNA kvantifisering, konfokalmikroskopi (CLSM) og fluorescensspektroskopi. Den optimaliserte formuleringens evne til å hemme- og eliminere biofilmer ble evaluert via farging med krystallfiolett og isotermisk kalorimetri (ICM). Toksisiteten av formuleringene ble evaluert mot HaCaT celler. De to modifiserte nanopartiklene NMC og NNP^{Chi} hadde en gjennomsnittlig størrelse på 22,3 ± 1,3 nm og 297,0 ± 2,9 nm, og et zeta-potensial på -24,2 ± 3,2 mV og +30,9 ± 1,0 mV. Begge nanopartiklene hadde høy grad biofilm gjennomtrenging i sammenlikning med kontroll formuleringen (52,5 ± 10,4 nm and -21,5 ± 3,5 mV). NMC ble valgt som kandidat for inkorporering av polymyksin B (PMB) på grunn av dets fordelaktige morfologi, størrelse og affinitet til PMB. Den optimaliserte PMB formuleringen hemmet effektivt *P. aeruginosa* biofilm-vekst og hadde en signifikant påvirkning på tid til maks metabolsk aktivitet (+444 ± 50 minutter) og relativ metabolsk rate (20 ± 5%) i etablerte biofilmer. Toksisitetsstudier viste ubetydelig toksisitet.

Til konklusjon kunne kationisk overflate-modifikasjon og konjugering med kolesterol i stor grad øke biofilm gjennomtrengingen av DNA nanopartiklene. Den optimaliserte formuleringen med PMB inkorporert demonstrerte lovende effekt mot *P. aeruginosa* biofilmer.

Nøkkelord: DNA nanoteknologi; drug delivery systemer; biofilm penetrering; polymyxin B

TABLE OF CONTENTS

LIST OF TABLES

LIST OF FIGURES

ABBREVIATIONS

AMR	Antimicrobial resistance
CV	Crystal violet
CLSM	Confocal laser scanning microscopy
DDS	Drug delivery system
DLS	Dynamic light scattering
DMEM	Dulbecco´s Modified Eagle´s Medium
DMSO	Dimethyl sulfoxide
DNA	Deoxyribonucleic acid
EB	Encapsulation buffer
EE	Entrapment efficiency
EPS	Extracellular polymeric substance
EPR	Enhanced permeability and retention
FBS	Fetal bovine serum
HGT	Horizontal gene transfer
IMC	Isothermal microcalorimetry
kDa	Kilodalton
LPS	Lipopolysaccharide
MDR	Multidrug resistance
MTT	3-(4.5-dimethylthiazol-2-yl)-2.5-diphenyltetrazoliumbromide
MHB	Mueller Hinton Broth
NIR	Near-infrared radiation
OD	Optical density
PBS	Phosphate-buffered saline
PMB	Polymyxin B
PDI	Polydispersity index
ROS	Reactive oxygen species
SD	Standard deviation
TEM	Transmission electron microscopy

1 INTRODUCTION

1.1 Antibiotic resistance

Over the last two years, society has been reminded of how detrimental a wide-spread, hard to treat infectious disease can be for the world. The COVID-19 pandemic serves as a reminder of how fragile and ill-prepared health care systems are against pathogens that cause severe diseases. The discovery of antimicrobial agents in the 20th century has revolutionized medicine, saved millions of lives from deadly microbial diseases, and contributed to extending the expected life span of the global population (1, 2). As such, retaining the efficacy of antibacterial agents can hardly be overstated. However, decades of mis- and overuse both in agriculture and public health has led to the alarming threat that is antimicrobial resistance (AMR). This concept has become a worldwide phenomenon and refers to a pathogen´s ability to resist antibiotic action to which it was previously susceptible. Today, AMR is declared a global public health concern, and there´s a dire need for more options in our arsenal to combat AMR. The emergence of antimicrobial resistance is not a novel subject, as Alexander Flemming, who discovered the first effective antibiotic, had already warned against overuse in the 1940s (3). A recent study estimated that as many as 10 million deaths could be attributed to AMR by 2050, overcoming mortality rates associated with cancer and stroke (4). The development of bacterial resistance is an unavoidable evolutionary process which can be slowed down but not completely halted (3). This arises from changes in the bacterial genome under selective antibiotic pressure, favoring the emergence of resistant strains (5).

Several mechanisms have been reported in association with AMR. For instance, the presence of efflux pumps (where clinically relevant antibiotics are exported from the bacterial cell), modification of the antibiotic´s target molecule, production of enzymes that inactivate the antibiotic, and the formation of **biofilms** are widely implicated in AMR (6). Bacteria can acquire genes coding for these protective mechanism via two main strategies: mutations in genes and the acquisition of genes coding for resistance mechanisms through horizontal gene transfer (HGT). In the scenario of mutational resistance, a portion of bacterial cells from a population susceptible to a given antibiotic will develop mutations in genes which affects the activity of the agent (7). This now resistant subset will outlive the susceptible population in the presence of the antibiotic, over time making the resistant bacteria dominant.

The acquisition of foreign DNA through HGT is one of the most important drivers of resistance that is known to distribute resistant genes. HGT is classically divided in 3 primary strategies for distribution of genetic material, **1**) conjugation, **2**) transformation and **3**) transduction, where the acquisition of free DNA through transformation is the least common (7). Conjugation is an especially efficient strategy for genetic exchange in bacteria, relying on cell-to-cell contact to transfer genetic material with the help of mobile genetic elements (MGEs) as vehicles such as plasmids (circular extrachromosomal DNA) as vehicles (7). The strategies allow susceptible bacteria to acquire antibiotic resistance from a donor bacterium in the surrounding area. Moreover, this gene transfer is not limited to bacteria of the same species, and therefore a multidrug resistance (MDR) gene can be shared to different species. In addition to the exchange of resistance-bearing genes, many bacteria can form biofilms. Biofilms do not only protect the bacteria against antibiotics and other environmental factors, but several studies have demonstrated that bacteria within biofilms exchange antibiotic resistance genes (ARG) much more frequently through HGT than between planktonic cells (8). This is because bacterial cells within a biofilm attaches to a matrix and are closely located together. Through the accumulation of resistance genes, the ability of MDR infections to resist multiple antibiotics is further enhanced by their ability to form biofilms and represent the most threatening infections to public health.

1.2 Biofilm infections

The relevance of structured and- tight-woven communities of bacterial, termed biofilms in medical microbiology is relatively new, first appearing in publications during the mid 1970s. Hoiby and coworkers acknowledged this grouping of bacteria in 1975, describing the chronic colonization of the respiratory tract with aggregations of *Pseudomonas aeruginosa* in cystic fibrosis patients (9). Since then, studies on biofilm formation and its role in clinical infections has increased in an exponential manner (**Figure 1**)

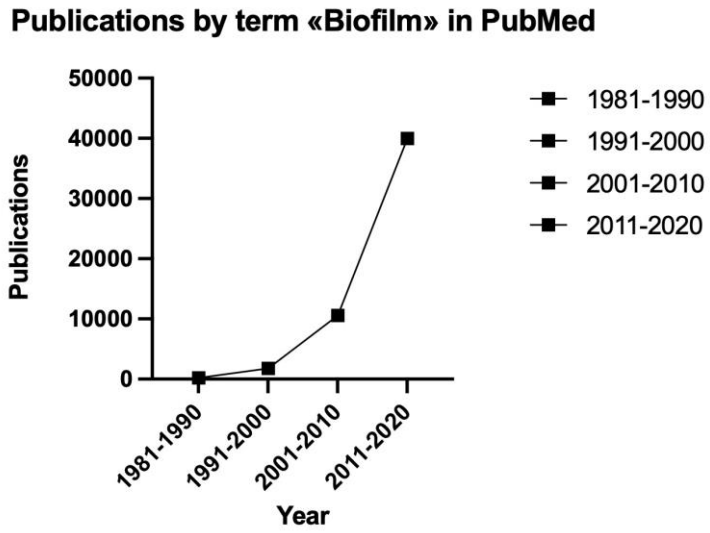

Figure 1: *Cumulative number of PubMed-listed publications in 10-year increments (search conducted 4th January 2022) (https://pubmed.ncbi.nlm.nih.gov/).*

In the biomedical context, biofilms are defined as an organized aggregate/network of microorganisms living within a self-produced extracellular matrix, attaching the community of bacteria to a surface, biotic or non-biotic (10). In general, bacteria can alternate between planktonic form and biofilm form, the latter being the preferable, natural form and presents several advantages to the embedded microbe. The formation of biofilm is commonly considered to occur in four sequential phases: (1) bacterial adherence on surfaces or aggregation on tissues, (2) microcolony formation with the production of extra polymeric substances (EPS), (3) biofilm maturation and differentiation and (4) detachment and dispersal of the bacteria (**Figure 2)** (11, 12). These microbial communities promote the survival of microorganisms in several different ways. First, biofilms assure stability against washing by water flow or blood stream, as fimbriae and flagella on the bacteria will keep the bacteria mechanically attached to the surface and to each other (13). Moreover, biofilms provide protection against harsh host conditions. As an example, consider the strong and repeated force an oral biofilm (dental plaque) must endure, whilst being subjected to the flow of water and food intake. In addition, the proximity and high cell density of bacteria embedded in biofilms for longer periods of time provides an optimal environment for the transfer of genetic material. Savage *et al* concluded in their 2013 study of the transfer of genes carrying antibiotic resistance in *Staphylococcus aureus* that the rate of conjugation was dramatically increased in the biofilm state as opposed to their planktonic state (14).

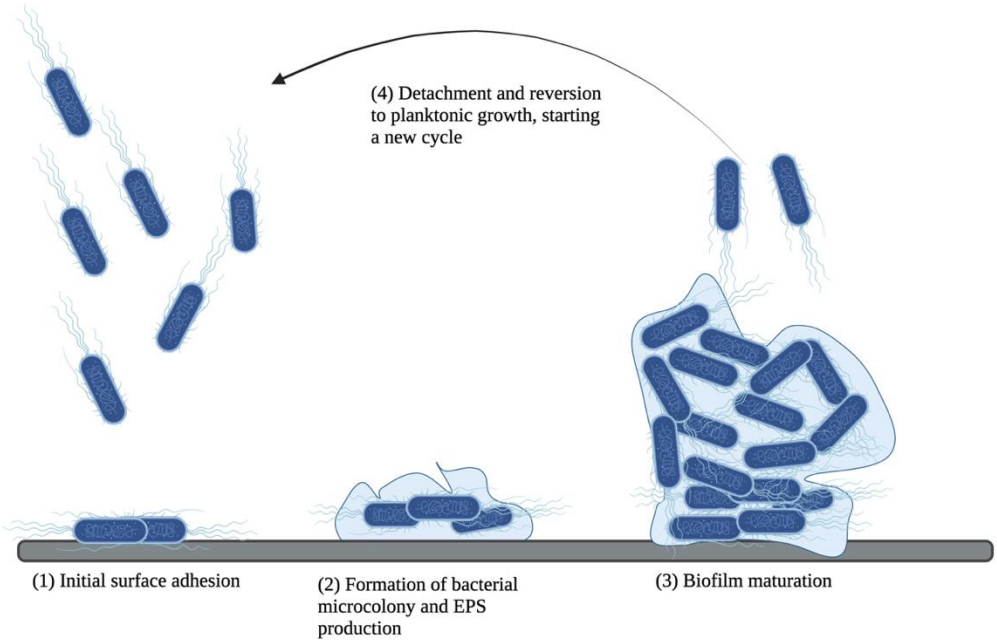

Figure 2: *Biofilm formation stages.*

Mechanisms that protect microbial cells within the biofilm from antimicrobials will be briefly explained in this section. However, the relevance of the extracellular polymeric substance (EPS) will be separately discussed due to its relevance to the thesis.

A typical mature biofilm contains large, anoxic regions, where studies have shown that in a 210 μm thick biofilm, oxygen penetrated only about 50 μm deep (15). This trait implies that portions of the bacteria in mature biofilms have limited access to oxygen and consequently limited metabolic activity. This reduced metabolic activity also implies a slower growth and division rate, reducing the efficiency of any therapeutic agents that target cell division (13). As demonstrated by Giorgia and coworkers, oxygen deprivation significantly reduced the efficiency of several antibiotics tested on both mature and 4-h old biofilms (15). In addition, essentially invulnerable bacterial cells, persister cells, have been found to comprise a small cell fraction. These persister cells lay dormant, with close to no metabolic activity, rendering inefficient every antibiotic that targets any of the processes relevant for cell growth and division. Such cells function as a reserve for reinfection and are thought to be a major contributor to the pathogenesis of chronic infections (13, 16, 17). In addition to these metabolic changes, several genes coding for efflux pumps are reported to be heavily upregulated in

biofilms, resulting in increased transportation of antibiotics from inside the cells, reducing their efficiency and providing the need for higher antibiotic concentrations (13, 18, 19).

Bacterial biofilms are now considered a serious health threat, as the formation of biofilms serves as a great challenge for antimicrobial therapy. The existence of persister cells contribute to the development of recurrent and chronic infections. Low metabolic activity dramatically reduces the effectiveness of drugs targeting cell replication and antimicrobials have limited traversal through a complex network of biopolymers and are prone to enzymatic degradation throughout their traversal. Biofilm infections account for a large part of the total infections (65% of all microbial infections and 80% of all chronic/recurrent infections) and are reported to inhabit upwards of 1000-fold resistance to antibiotics compared to their planktonic counterpart (10, 20). Throughout the last 20 years, a lot of knowledge has been gathered on the subject, and as we acquire more, the need for new, novel approaches to combating biofilms are as clear as ever.

The mechanisms accounting for the increased tolerance and the benefits of being in a biofilm are summarized in **Table 1**.

Table 1: *Mechanisms by which biofilms favor bacterial survival.*

Mechanism	**Method of increased tolerance**
Increased tolerance to harsh host environments	Bacterial protection against the flow of water and blood, allows the cells to stay alive for longer than planktonic bacteria under mechanical stress.
Low metabolic activity	Areas of the biofilm experience low access to both nutrients and oxygen, making some bacteria enter a low-activity state with reduced metabolic activity. This renders antibiotics targeted at cell replication less efficient.
Persister cells	The presence of difficult to treat dormant bacterial cells serves as a disease reservoir.

EPS matrix	The secreted EPS matrix from the bacteria functions as a physical barrier in which several molecules can´t penetrate through.
Horizontal gene transfer	Increased rate of gene transfer through conjugation due to bacterial proximity, promoting the emergence of resistant bacteria.

1.3 The EPS matrix

In the context of bacterial protection in biofilms, the EPS matrix plays a detrimental role on the penetration of foreign bodies such as antibiotics and nanoparticles. The EPS matrix, or as Hans-Curt Flemming metaphorically termed "The house of the biofilm cells", is a collection of different biopolymers produced by the bacteria and in which they become embedded in (21). These biopolymers include polysaccharides, lipids, proteins and extracellular DNA and make up most of the dry mass of the biofilms (accounting for more than 90% of the total biofilm weight) (22).

Extracellular proteins represent a large mass portion (by mass) of the biofilms with several important structural functions, including several enzymes, which turns the matrix into a digestive system by breaking down proteins, lipids, DNA and other organic compounds into nutritional factors for bacterial cell growth (130). These enzymes are also in part responsible for the detachment of the bacterial cells in the biofilm in the growth cycles. Matrix structural proteins play several diverse and important roles in the formation of biofilms. By mediating the initial surface attachment, cell-cell adhesion and cell-carbohydrate/matrix interaction, they are a key part of the formation- and stabilization of biofilms (23)

Exopolysaccharides is another important constituent of the EPS matrix that contributes to a large portion of the biofilm matrix by dry mass (22). For many biofilm-forming bacteria, the production of exopolysaccharides is indispensable to the formation of strong three-dimensional biofilms. Whilst still capable to some degree, mutants of biofilm-forming bacteria which cannot synthetize exopolysaccharides have shown limited biofilm forming potential. In general, the

exopolysaccharides make up the “sticky” part of the biofilms, serving as scaffolds, providing binding sites for the other EPS components and other bacterial cells to adhere, contributing heavily to the biofilm cohesion (24). Moreover, the tight polysaccharide network of the matrix poses a considerable challenge for carriers seeking to penetrate it by interacting with the nanocarriers (25). Whilst most polysaccharides are not biofilm specific, the composition and portion vary a lot between different strains, stress experienced, available nutrition and environment (26). Albeit many of the exopolysaccharides serve structural purposes, some exopolysaccharides also serve as important virulence factors associated with disease, vital for the bacteria’s pathogenicity (27).

The role of extracellular DNA (eDNA) in the formation and upkeep of biofilms were until the early 2000s believed to be slim. However, since then, several studies have proved the importance of the eDNA in several strains (28, 29). There is an abundance of DNA found in the biofilms of several bacteria. The origin of this DNA is most importantly, but not excluded to, the lysis of bacterial cells by its own enzymes, releasing the DNA contained in the cell (autolysis) (30, 31). Like exopolysaccharides and proteins, eDNA plays a role in cell-to-cell adhesion and stabilization of the biofilm 3D architecture (32). Although double stranded DNA is an amphiphilic molecule, several studies suggest that an abundance of eDNA increases the hydrophobicity of the bacterial cell surface, enhancing the adhesion to other hydrophobic surfaces, facilitating adhesion to abiotic surfaces (31). In addition to its role in the early-stage adhesion and aggregation, eDNA is directly responsible for the vast, easy-accessible gene-pools many biofilms have in contrast to the other EPS constituents. Moreover, being a polyanionic molecule, DNA can bind to cations seeking to penetrate to the bacterial cells, protecting them against cationic antibiotics and peptides produced by the immune system (31). The polyanionic nature of the DNA further protects the bacteria against other negatively charged molecules through electrostatic repulsion. The role of the different biopolymers can be seen summarized in **Table 2**

Table 2: *EPS functionalities.*

EPS component	**Function**
Polysaccharides	Biofilm cohesion & structural integrity

	Protective barrier against foreign bodies Nutrient source Sorption
Structural proteins	Biofilm cohesion and structural integrity Protective barrier against foreign bodies Nutrient source Sorption
Enzymes	Enzymatic activity, breaking down biological molecules for carbon, nitrogen and phosphate sources
eDNA	Biofilm cohesion Nutrient source Protective barrier against foreign bodies Gene-pool

The broad-spectrum activities of polysaccharides, DNA and proteins and their interactions with particles seeking to penetrate the biofilm inevitably attaches a biomolecular corona to the particle ("coating" of biomolecules on the surface) thereby altering the particles surface properties and ultimately affecting particle-biofilm interaction. Therefore, to traverse this network of biopolymers, antimicrobial agents can advantageously be incorporated in carriers with enhanced properties to ensure the agent reaches the desired target site.

1.4 Nanomedicine as an antibiofilm strategy

Conventional therapy against biofilms lacks the desired efficacy, and the development of alternative therapeutic agents is an extremely time-consuming process, further affected by

regulatory, societal and economic factors. As an example, several pharmaceutical companies have opted to invest less in the antibiotic field as a result of low returns on their large investments (33). To address the dried antibiotic pipeline, several incentives for the research and development of antimicrobial agents have been created and new antibacterial strategies have emerged in the last decades (34). One of the most promising fields, expanding to several other biomedical areas (such as cancer therapy, diagnostics, vaccines, etc.) is the nanomedicine area. Nanomedicine is the application of nanotechnology for both treatment and diagnostics of diseases. Nanosized materials are commonly classified as particles with a diameter of 100 nm or smaller (35, 36). However, the term nanocarriers usually describe colloidal particles that vary in size from 10 nm to 1000 nm (37). A more field-specific definition proposed in 2000 was: "Nanotechnology is concerned with materials and systems whose structure exhibits novel and significantly improved physical, chemical and biological properties **due** to their nanoscale size" (38). The utilization of nanotechnology for medical purposes is identified as a Key Enabling Technology and is predicted to provide several innovative, improved medical solutions for both diagnostic- and treatment purposes (39). Some of the most reported nanoparticles are shown in **Figure 3** and includes inorganic particles (such as gold and silica), polymeric particles (for example chitosan and polyacrylate), lipid-based particles (such as liposomes and solid-lipid particles) and more recently, DNA-based nanoparticles.

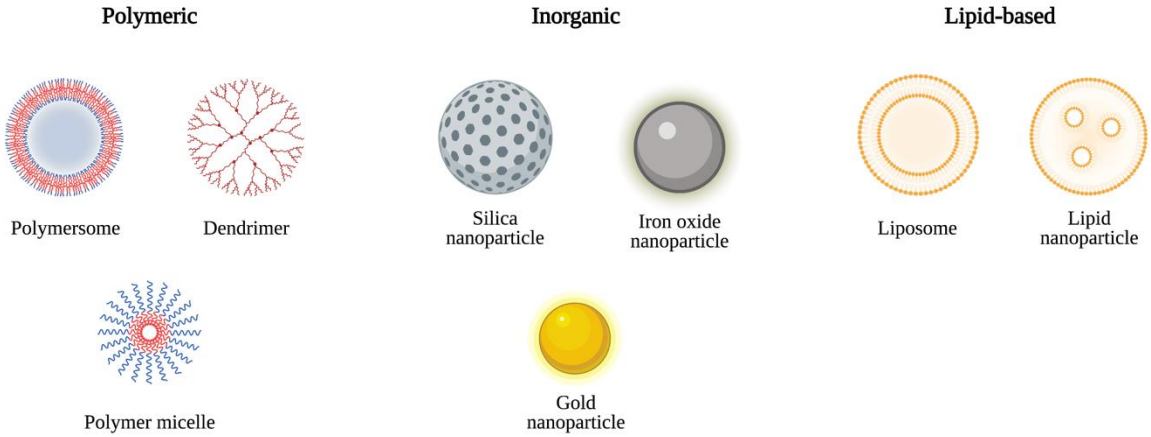

Figure 3: *Different classes of commonly reported nanoparticles.*

Delivery systems utilizing nanotechnology have been highly successful in the past decades in improving drug delivery and represent the most effective uses of nanomedicine today. As an example, liposomes have been used as platforms for cancer therapy in the FDA approved Doxil ® formulation since 1995. In this formulation, doxorubicin is encapsulated in a liposome, providing enhanced drug accumulation at site of disease, protection and reduced toxicity (40, 41). In cancer, the use of nanocarriers has improved the pharmacokinetics of several drugs, accompanied by a reduction in toxicity. The magnitude of the nanoparticles increased accumulation at the site of disease has been reported to be upwards of 10-50-fold compared to free drug when injected (0.01% to 1-5% for nanoparticles) (42). This increased accumulation is due to a phenomenon termed the "enhanced penetration and retention (EPR)" effect. In short, the vasculature of tumors and other inflamed tissue are comprised of poorly aligned, defective endothelial cells with wide gaps, making the inflamed tissue more prone to extravasation and retention of nanocarriers (43).

In recent years, nanotechnology has gained a great deal of interest as a tool for antibiofilm applications due to their superior features, seeking to replicate the success found in cancer therapy drug delivery. Nano systems offer a wide variety of advantages as drug delivery systems for antimicrobials, such as cargo protection, increased stability, better solubility, optimization of surface-properties to ensure efficient delivery of antimicrobial cargo and improved interaction with microbial membranes (44). The tuneability of nanoparticles allow for the manipulation of nearly every physical characteristic making them very versatile, endowing the particles with desired properties that can increase the efficiency of drug delivery. Additionally, some nanomaterials exert unique properties such as near-infrared-radiation (NIR) to heat capabilities, possessing antimicrobial activity themselves (45). This enables the use of dual-purpose drug delivery systems that can effectively disrupt biofilms synergistically through several mechanisms.

In the antibiofilm context, several papers have been published utilizing different nanomaterials that demonstrate the capability of optimized NPs to penetrate and aid eradication of biofilms (46, 47). Some of the antibiofilm applications of nanomedicine is summarized in the **Table 3.**

Table 3: *Antibacterial applications of nanomedicines (131-136).*

Approach	Mechanism	Advantage
Drug delivery systems	Utilization of nanomaterial as drug carriers	Improved accumulation and penetration of drugs, the potential of active targeting, increased interaction with the bacterial cells embedded in the biofilm, protection against the matrix components (including enzymatic degradation). Allows for combination-therapy utilizing several anti-biofilm mechanisms
Photothermal therapy	Utilization of nanomaterials capable of converting light to heat under NIR irradiation, generating a local bactericidal hyperthermia	Very efficient eradication of established biofilms (48-50), easily controllable parameters (temperature, density, time). Nanomaterial functioning as both photothermal agent and carrier opens for dual-approach therapy in one system.
Photodynamic therapy	Generation of reactive oxygen species, killing the bacteria and disrupting the biofilm	ROS generation functions toward both the bacterial cell and the EPS matrix
Nanozymes	Nanoparticles carrying intrinsic peroxidase-like activity, producing ROS which disrupts biofilm	ROS generation functions toward both the bacterial cell and the EPS matrix,

1.5 Enhancing biofilm penetration through nanocarrier design

The interaction between a given nanoparticle and a bacterial biofilm can be regarded in three main steps: (1) transport to the biofilm vicinity, (2) attachment to the biofilm outer surface and (3) migration within the biofilm EPS matrix, with the most important interactions between the

NP and the EPS matrix being electrostatic-, hydrophobic- and steric (51). All these stages and the efficacy of the migration is heavily dependent on the physiochemical properties of the nanoparticle. Consequently, the penetration of nanoparticles depends on several factors, such as surface charge, surface composition, size, shape and bacterial factors like biofilm maturity. The use of nanocarriers enables fine tuning of these properties to promote a preferential migration of particles through the biofilm. In this section, the importance of selected physiochemical properties regarding antimicrobial activity and biofilm penetration will be reviewed, and an overview of their impact on NP-biofilm interactions will be discussed.

1.5.1 Size

The size of nanomaterials plays a detrimental role in determining the materials properties and performance in biomedical applications (52). Nanomaterials are the size where material sciences meet biology, and as such, their size is directly implicated in how the nanoparticle interacts with cells and other entities. In this context, interactions with cells often require certain size restrictions due to steric effects during binding interactions. Nanotherapeutics rely on effective cellular uptake and permeability which means that optimum interactions between the carrier and cell becomes a size-dependent matter (53). Additionally, the size of the nanocarrier have implications in antibiofilm therapy. Peulen and coworkers have demonstrated the effect of size on particle diffusion through P. *aeruginosa* biofilms (54). In this work, they found that nanoparticles of 50 nm sizes travelled faster through the pores of a biofilm. They concluded that the diffusion coefficient decreased exponentially with the square radius of the nanoparticle, implying that smaller NPs typically penetrate biofilms more readily. Similarly in a different work, Nallathambi and coworkers compared the effect of NP diameter on cell internalization in P. *aeruginosa* (55). In this work, they found that the smaller NP (13 nm) had a higher intracellular concentration than the larger (90 nm), and that there was a size-dependent efflux pump activity. Furthermore, works have been published which reporting that NPs with a size upwards of 300 nm could readily penetrate *P. aeruginosa* biofilms, whilst larger NP (1000 nm) could not (56). In summary, it can be concluded that there is an ideal diameter range for NP seeking to penetrate P. *aeruginosa* biofilms from 10 nm to 300 nm, but not exceeding 1000 nm and that the ideal size is not necessarily the same for all materials and biofilm conditions.

1.5.2 Surface charge and hydrophobicity

For effective drug delivery, cellular uptake is usually a prerequisite and is governed in addition to size by the surface chemistry like hydrophobicity and charge (57). Specifically, positively charged particles have been demonstrated to interact in a larger degree with bacterial cells, owing to their negatively charged membrane, increasing the efficacy of drug delivery. By virtue of this fact, cationic particles have also been seen to exert higher toxicity than anionic particles. Additionally, the surface charge and hydrophobicity of the nanoparticle has been demonstrated to be directly implicated in the traversal through biofilms. Rotello and coworkers demonstrated the importance of surface charge on biofilm penetration in their 2015 work, where they prepared quantum dots (QD) with different properties to explore the effect biofilm penetration (58). In this work, equally sized quantum dots were prepared as cationic, anionic or neutral particles. After 1 hour incubation, no quantifiable amount of the anionic and neutral QDs were found within the EPS matrix or bacterial cells, indicating the absence of biofilm penetration for these formulations. In contrast, the cationic QD could effectively penetrate the bacterial biofilm with quantifiable amounts inside the EPS matrix and bacteria cell. The authors also noticed a difference in localization for hydrophilic and hydrophobic particles. The hydrophobicity of the NPs had a markedly effect on the localization of the cationic QDs. Whilst the hydrophilic cationic QD could effectively penetrate the EPS matrix but were not in a large degree internalized in the bacterial cells. The hydrophobic cationic QDs were more homogenously distributed throughout the biofilm than their hydrophilic analogs, and in a much larger degree, internalized in the embedded cells. Additionally, Alhajan and coworkers incorporated an antimicrobial agent in both negatively- and positively charged liposomes and evaluated their effect against *P. aeruginosa* biofilms (59). In this work, the positively charged liposomes were much more effective than their negatively charged counterpart, which they concluded was a result of a higher degree NP-biofilm interaction. Conversely, negatively charged nanoparticles have also been found to penetrate biofilms (60). However, these carriers required long incubation with the formulation (i.e., 24 hours). Overall, positively charged NPs have been found to interact with the components of the EPS matrix and bacterial cell. However, this fact also implies that cationic NPs will also interact with healthy cells, possibly increasing the toxicity of the formulation (59).

1.5.3 Shape

Being directly related to the surface area and NP-cell interaction, the shape of the NP can have a profound effect on its antibacterial properties. Shape-dependent cellular uptake and antimicrobial efficacy of nanoparticles has been widely demonstrated in literature. For instance, Penders and coworkers prepared a series of gold NPs with different morphology (nanoflowers, nanospheres and nanostars) and tested the antibacterial efficacy against S. *aureus* (61). In this work, they found that the shape significantly altered the antibacterial properties of the NP, with the nanoflower showing the highest efficacy. The authors attributed this to the increased surface area of the nanoflowers and consequently higher probability of NP-cell membrane interaction. Nano-knives of graphene oxide is a novel approach to combat MDR superbugs having showed promising results (62). For this NP, the shape is believed to be a major factor in the antibacterial effect, as the sharp edges can puncture bacterial cell walls upon contact, causing leakage of intracellular components and consequently cell death.

1.6 DNA nanotechnology

Deoxyribonucleic acid (DNA) is the macromolecule carrying the genetic material in all living organisms, and functions as a tape carrying the information for protein synthesis (63). DNA consist of two polynucleotide chains covalently bound to one another; each being composed of nitrogenous bases that are supported by sugar-phosphate backbones. Through complementary base-pairing, the nitrogenous bases will bind to one another to form the DNA double helix. The nitrogenous bases in DNA are guanine, cytosine, thymine and adenosine, and will bind only to their complementary base, wherein cystine binds to guanine – and thymine binds to guanine. This base pair mechanism is the foundation for the bottom-up production of DNA structures, allowing for the design of DNA-based nanomaterials through the rational design of specific base sequences. “Bottom up” synthesis is one of two major approaches of producing NPs. This approach is based on the exploitation of building blocks properties to direct a self-organization without external force. In DNA nanotechnology, this process is called DNA self-assembly, and is based on “sticky-end” cohesion, where motifs containing complementary base pairs hybridize to form structures (64). This molecular recognition which the base-pairing provides allows for unparalleled control over the size and physical properties of the structures. The journey in utilizing our genetic material as scaffolds began in a pioneering 1980 paper, when Ned Seeman proposed that DNA could be utilized as a framework to crystallize

macromolecules (65). Using single stranded overhangs, sticky ends, he formed immobile junctions, which could be coupled together to produce lattices (65, 66). In this way, he concluded that he could with great specificity engineer lattices with a high degree of predictability. Two decades after the first papers in the field, Zheng, Seeman and coworkers used a clever design to self-assemble a 3D DNA crystal, effectively proving the potential of DNA to self-assemble into novel structures (67). There are generally two main design techniques to develop nanostructures, tile- and origami-based approaches (64, 68). In the first, DNA tiles bind to complementary sequences for the generation of a specifically designed carrier (69). In the origami technique, a scaffold (single strand of DNA up to several thousand nucleotides long) is folded by many shorter, complementary strands that assemble to the desired shape (64, 70). Using the mentioned strategies, several 2D and 3D structures have been developed (64). **In Figure 4** some of the more common DNA nanocarriers are depicted.

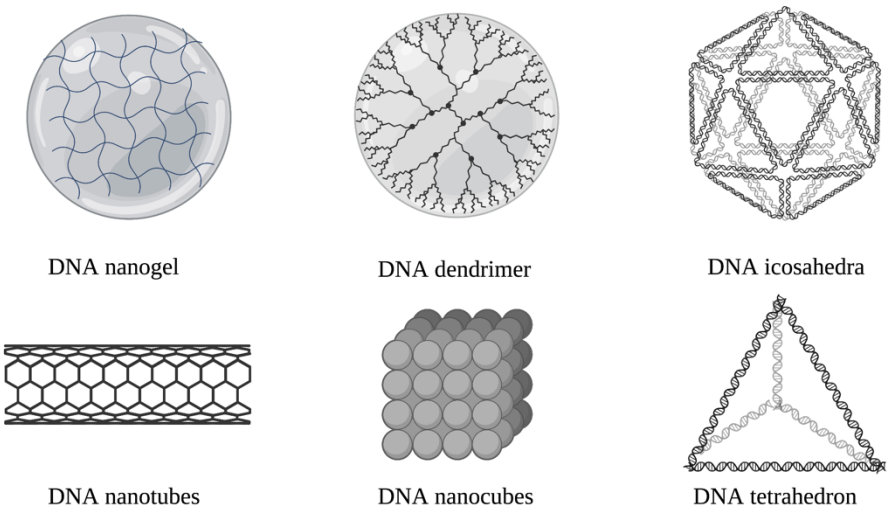

Figure 4*:* Different DNA nanostructures.

Due to the progress in using DNA for rational carrier development in the last decade, DNA nanostructures have been proven to be promising candidates for drug delivery against bacterial

biofilms. Being a natural occurring macromolecule, DNA is inherently biocompatible and degradable. This excellent biocompatibility has been demonstrated in several research articles and provides an advantage over other NPs utilizing inorganic materials which often pose toxicity concerns and uncertain *in* vivo fate (71, 72). The same works have also established the low immunogenicity of nucleic acid-based NPs. Several developed DNA nanocarriers have demonstrated high cellular uptake of the internal cargo, such as small-molecule drugs, photosensitizers, antimicrobial peptides and more (73). For instance, DNA-based hybrid systems have demonstrated to promote the uptake of antibacterial agents in an efficient manner. Magdiel and coworkers developed a novel theranostic platform utilizing a self-assembled DNA product as a scaffold for the incorporation of an antibacterial agent, which could effectively transport the agent over the bacterial membrane (74). This platform was also functionalized with conjugated gold clusters, to impart the nucleic acid-based NP with trackability. Additionally, by leveraging on the repulsion between DNA NPs and bacterial cells, a recent study demonstrated the use of DNA NPs as an antifouling strategy that hinders the establishment of bacterial biofilms (75).

Despite the promising ability of using DNA nanoparticles as therapeutic weapons in combating microbial infections and biofilms, some limitations are present. One example is the high cost of developing sophisticated and complex DNA nano systems, as the raw materials, synthetic DNA, come at steep price - more than that of most commodity chemicals (76). Additionally, the carrier stability can be impaired due to the presence of deoxyribonucleases (DNA-degrading enzymes) in serum and biofilms that can induce carrier degradation prior to reaching the target. Furthermore, DNA nanoparticles are prone to the opsonization effect, where adsorption of non-specific proteins in serum marks the carrier for uptake by macrophages (77). Additionally, the polyanionic nature of unmodified DNA limits interaction with the negatively charged EPS matrix of biofilms and bacterial cell membrane due to electrostatic repulsion which can potentially cause inefficient delivery of cargo. Nevertheless, rational modification of nucleic acid-based NP can be pursued to address these challenges.

1.6.1 Modification of DNA nanoparticles

Nucleic acid-based NPs can be modified in several ways, through cargo conjugation, base sequence modification and surface coating to endow the NP with enhanced physiochemical properties for antimicrobial purposes

For instance, the fabrication of DNA amphiphiles by connecting a hydrophobic moiety to DNA strands increases the overall hydrophobicity of the self-assembled product (78). This enables the incorporation of both hydrophobic and hydrophilic drugs giving access to a wide arsenal of antimicrobial agents (68, 79). Furthermore, the increased hydrophobicity enhances the insertion into membranes and promotes uptake into mammalian cells (80). The interaction between the cationic natural polymer chitosan and DNA is now well established (81). By leveraging the electrostatic interaction between chitosan and DNA, DNA can be coated with the polymer to increase the surface potential of the nanocarrier. This has potential benefits of enhancing biofilm penetration via interactions with the biofilm matrix and bacteria cell wall. The coating of DNA with chitosan can also endow the NP with a synergistic antimicrobial effect, as the antimicrobial effect of chitosan itself has been widely reported (82).

Furthermore, conjugating DNA based NPs with other organic and inorganic materials (proteins, lipids, gold, silver, etc.) enhances the stability of the carriers against enzymatic degradation, increases functionality, enhances cellular uptake, controls drug release and increases binding to bacteria membranes (83-86). To further increase the stability of the nucleic acid-based NP, the phosphodiester bond (DNase´s target) can be modified to increases the resistance to DNase degradation (87). Such characteristic can be achieved via the synthesis of peptide nucleic acid (PNA) – a nucleic acid with a peptide backbone that can self-assemble to generate a product much more stable against DNase degradation (87, 88). Another strategy is to further encapsulate the DNA structure in another carrier, such as liposomes. Perrault and coworkers demonstrated in their 2014 paper that the encapsulation of a DNA nanostructure in lipid-bilayers protected it against DNase, lowered the immune activation after injection and increased the bioavailability several-folds in mice (89). In this work, the lipid bilayer encapsulating the DNA structure was further modified with polyethylene glycol, (a well-demonstrated approach to increase the circulation time in blood) to allow the platform enough time in circulation to reach the desired area of inflammation.

To address the challenges of treating biofilm infections, there is a need to develop innovative, biocompatible, and potent nanocarriers. Despite the benefits of DNA nanocarriers as advances systems, they suffer from daunting *in vivo* stability and limited interactions with EPS components and bacterial membranes. While literature has demonstrated that the modification of DNA carriers can enhance biological functions, this effect has been largely limited to cancer therapy. However, the pressing matter of AMR and emergence of hard-to-treat biofilm forming bacteria incentives the exploration of this nascent field for bacterial application.

2 AIM OF THE STUDY

Despite the potential benefit of DNA based nanostructures as antibacterial platforms, their characteristic anionic and hydrophilic feature makes transversal through biofilms or bacterial membranes a major challenge. There is therefore a need to identify new design approaches that can address this drawback. Therefore, the overall objective of this project was to develop an innovative DNA nanocarrier that can transverse the biofilm matrix and evaluate the capacity of the optimized system to deliver antimicrobial cargos. We envisioned this platform as an attractive system that can enhance the stability of antibiotics and overcome the limited penetration through the biofilm with minimal toxicity to tissues.

Herein, a series of DNA based nanocarriers were fabricated with varying sequence and surface modification. First, unmodified DNA sequences were designed and self-assembled into DNA nanogels (NNP) bearing anionic surface features and hydrophilic properties.

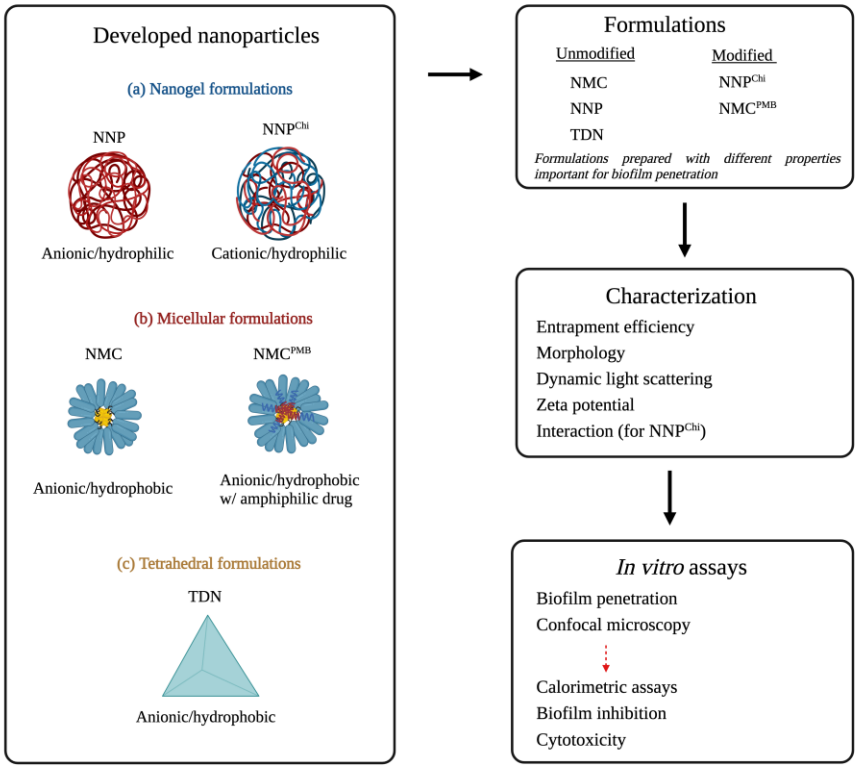

Figure 5: *Illustration of project plan and the developed nanoparticles.*

To investigate the role of surface modification, NNP was polymer coated with chitosan to develop hydrophilic DNA nanoparticles with cationic surface potential. Thereafter, large tetrahedral DNA nanoparticles with similar size as the chitosan coated nanoparticles were prepared as a control and compared with the chitosan coated nanoparticles. The impact of hydrophobic modifications was then investigated via covalent integration of cholesterol to prepare micellar DNA nanoparticles (NMC). Following characterization of the carriers, nanoparticle morphologies were visualized, and their biofilm penetration was then investigated to identify the optimized system. The micellar nanoparticle was identified with ideal physiochemical properties and biofilm penetration and was therefore further developed as a potential multifunctional platform against biofilm infections. To achieve this, polymyxin B was incorporated into the micellar system and the effect of drug concentration on the fabrication process, *in vitro* characterization, antibiofilm properties and toxicity was investigated.

3 MATERIALS AND INSTRUMENTS

3.1 Materials

All synthetic oligonucleotides were obtained from Integrated DNA Technologies, Inc (IA, USA) the sequences are listed in full in Table 4.

Table 3: *Sequences of ssDNA used in the fabrication of DNA nanogels (blue), micelles (orange) and tetrahedron (green).*

Code	Name	Sequence
YSAF	Y1-SAF	5´-GTCTTCGTCCTTATCGGTAGGGTGCTGAGCGGAATC CTGA-3´
	Y2-SAF	5´-GTCTTCGTCCTTTCAGGATTCCGCTCAGTCATGTCATCAC -3´
	Y3-SAF	5´-GTCTTCGTCCTTGTGATGACATGACACCCTACCGAT-3´
	Y3-SAF_FLUOR	5´-Alex594N-GTCTTCGTCCTTGTCCAACCGCTATCGCATCTCATG-3'
YSAB	Y1-SAB	5´-ATCGGTAGGGTGCTGAGCGGAATCCTGA-3´
	Y2-SAB	5´-TCAGGATTCCGCTCAGTCATGTCATCAC-3´
	Y3-SAF	5´-GTCTTCGTCCTTGTGATGACATGACACCCTACCGAT-3´
LAC	L1-SAC	5´-AAGGACGAAGACGTAGCCTACTATCTTCATTACCAGGTGCAGCC-3´
	L2-SAC	5´-AAGGACGAAGACGGCTGCACCTGGTAATGAAGATAGTAGGCTAC-3´
Micelle	M1C_chol	5´- ATCGGTAGGGTGTCA/3CholTEG/-3´
	M1C_c_fluor	5'-RhoR-XN-ATCGGTAGGGTGTCA-3CholTEG-3´
Tetrahedron	T1	5´-A GTC TTC GTC CTT ATC GGT AG A GGT GCT GAG CGG AAT CCT GA A AGT GTA CAA GGT ATC TCG AC-3´
	T2	5´-A CTA CCG ATA AGG ACG AAG AC A CTA AGA CTG GAG GAC CGA TG A CGA GCA GAC AAC AGC GC-3´
	T3	5´-A TCA GGA TTC CGC TCA GCA CC A GCG CTG TTG TCT GCT CG A ATG TAC CAT CGT TAC TAG AT-3´

T4	5´-A CAT CGG TCC AGT CTT AG A GTC GAG ATA CCT TGT ACA CT A ATC TAG TAA CGA TGG TAC AT-3´

3.2 Hardware and devices

- Zetasizer, Nano ZS, Malvern Instruments Ltd (Malvern, UK)
- Transmission electron microscope model HT7800, Hitachi Ltd (Tokyo, Japan)
- SPARK multimode microplate reader, Tecan Group Ltd (Männedorf, Switzerland)
- Confocal laster scanning microscopy model LSM 800, Zeiss (Oberkochen, Germany)
- NanoDrop One (c) Microvolume UV-Vis spectrophotometer, Thermo Fisher Scientific (Walthmam, MA, USA)
- Pierce 96-Well Microdialysis Plate MW cut-off 13.5 kDa, Thermo Fischer Scientific (MA,USA)
- CalScreener IMC device, Symcel (Stockholm, Sweden)
- T100 Thermal Cycler, Bio-Rad Laboratories (CA, USA)
- Gel Doc XR+, Bio-Rad Laboratories (CA,USA)

3.3 Software

All figures were created using the illustrator on the BioRender.com platform. Statistical analysis and graphs were carried out using Graphpad Prism version 9 (CA, USA). Statistical significance between the formulations were evaluated using two-sample student t tests and ANOVA analysis. The significance level used for the statistical analysis in this thesis was set at p=0.05. The calorimetric data was extracted using Symcel online analysis tool (https://symcel.com/analysis-tools/calorimetric-growth/)

4 METHODS

4.1 Preparation of DNA nanoparticles

The developed formulations with their respective hydrophilic or hydrophobic properties and surface properties are summarized in **Table 5**

Table 4: *Physical properties of the developed DNA nanoparticles.*

No.	Formulation	Group	Surface charge	Structural property
1	NNP	**Unmodified**	Anionic	Hydrophilic
2	NMC^{ss}		Anionic	Amphipathic
3	TDN		Anionic	Hydrophilic
3	NNP^{Chi}	**Modified**	Cationic	Hydrophilic
4	NMC^{Pmb}		Anionic	Amphipathic

NNP*: Nucleic acid nanogel*

NMC^{ss}*: Nucleic acid micelle (ssDNA)*

TDN*: Tetrahedral DNA nanoparticles*

NNP^{Chi}*: Nucleic acid nanogel (Chitosan)*

NMC^{Pmb}*: Nucleic acid micelle (Polymyxin B loaded)*

4.1.1 Preparation of monomers for nanogel fabrication

The DNA nanostructures YSAF, YSAB and LAC were prepared using an annealing process previously reported (90). In short, stochiometric quantities of the oligonucleotides shown in **Table 3** were added to a 10x encapsulation buffer (EB) (5 mM Tris-HCL, 1mM ethylenediaminetetraacetic acid (EDTA)) and DNase free water to achieve a working 1x buffer solution with the oligonucleotides. The single stranded DNA sequences were then subjected to a thermal annealing process, generating the three individual nanostructures needed to prepare the nanogel (**Figure 6)**. The concentration of the individual nanostructures was as follows: 4 μM Y-SAF, 1 μM Y-SAB and 6.5 μM L-SAC. For the annealing process, YSAB was heated at 95℃ for 5 minutes, 55℃ for 30 minutes, 37℃ for 30 minutes, 25℃ for 30 minutes and allowed

to cool for 30 minutes at 4℃. YSAF and LAC solutions were heated at 95℃ for 5 minutes, 60℃ for 30 minutes, 50℃ for 30 minutes, 37℃ for 30 minutes, 25℃ for 30 minutes and allowed to cool for 30 minutes at 4℃.

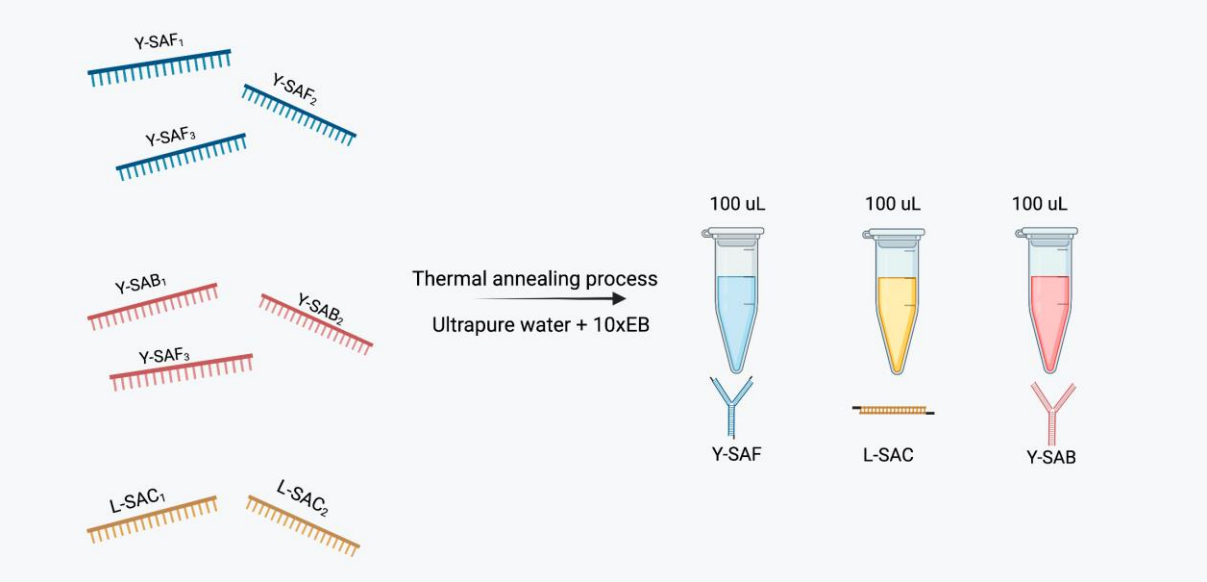

Figure 6: *Fabrication of DNA nanogel monomers through thermal annealing process.*

4.1.2 Preparation of blank DNA nanogels

The DNA nanostructures (YSAF, YSAB and SAC) was then mixed in equal volume and subjected to a second thermal annealing process (**Figure 7).** For this thermal annealing process, the nanostructures were heated at 95℃ for 5 minutes, 25℃ for 30 minutes and then allowed to cool at 4℃ for 3 ½ hours to prepare the blank DNA nanogel.

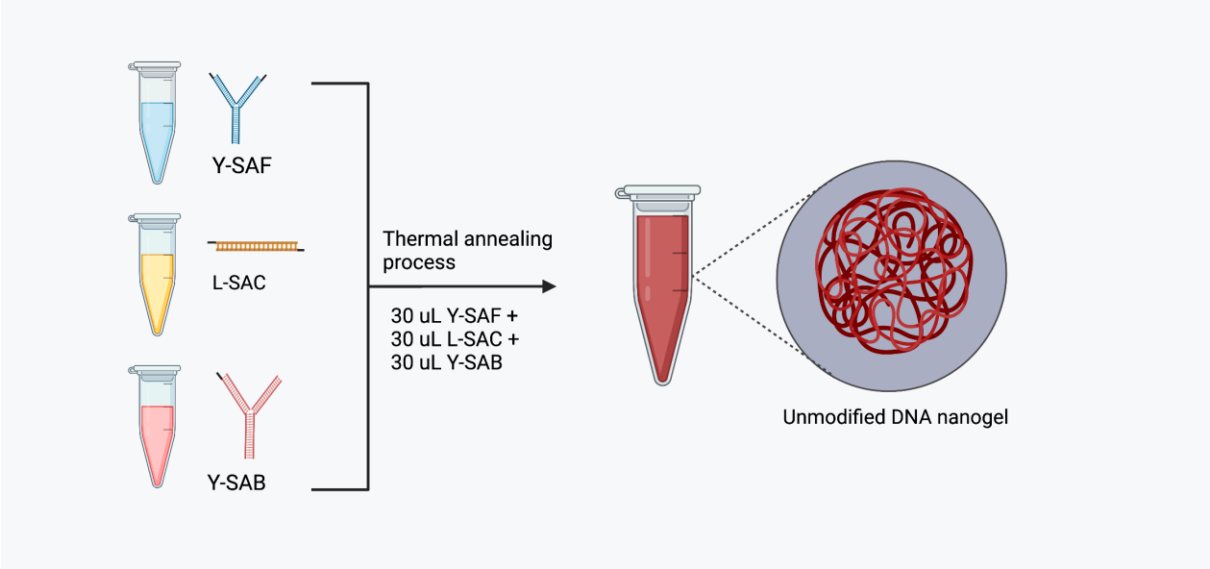

Figure 7*: Fabrication of unmodified DNA nanogels.*

4.1.3 Preparation of chitosan-coated DNA nanogels

To form the chitosan-coated DNA nanogel a stock chitosan solution was made by dissolving medium-molecular weight chitosan in 0.1% v/v glacial acetic acid. This solution was stirred over night at room temperature to assure that the chitosan was properly dissolved.

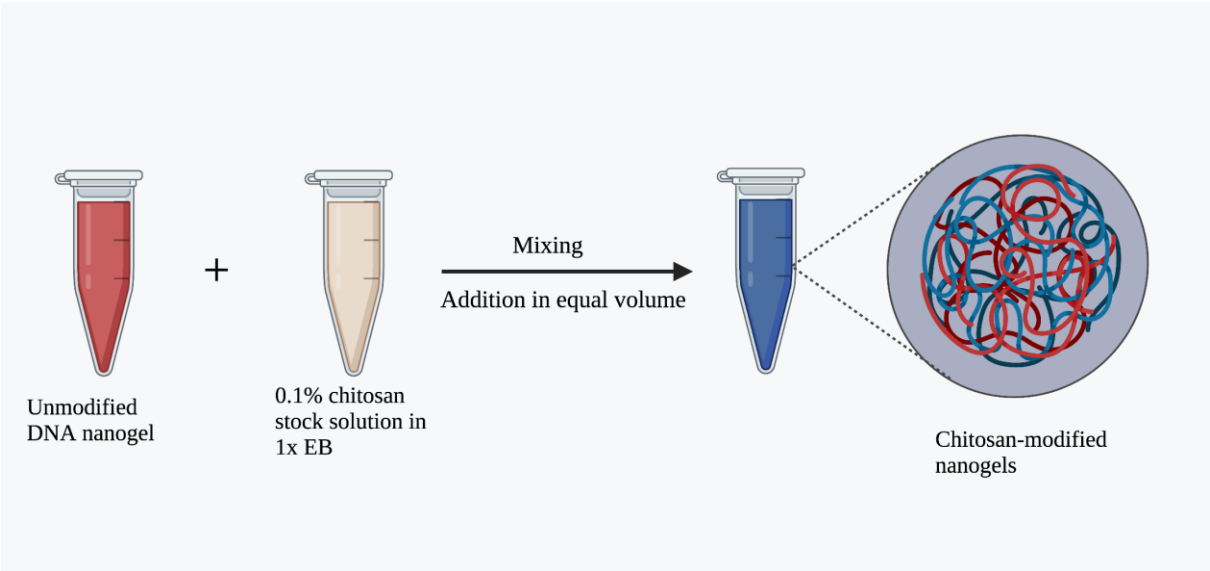

Figure 8*: Fabrication of chitosan-coated DNA nanogels.*

The chitosan stock solution was then diluted in 1x EB buffer to prepare a 0.1% w/v chitosan solution. The 0.1% w/v solution was then added in an equal volume to blank DNA nanogels, giving a final concentration of 0.05% w/v (**Figure 8)**. The interaction between the DNA nanostructures and the chitosan was assessed using electrophoresis. The chitosan concentration to be added in equal volume was decided through biofilm eradication assessment and effect on size **(Appendix Figure 1).**

4.1.4 Preparation of tetrahedral DNA nanostructures

To prepare the tetrahedral DNA nanostructures, four DNA strands were utilized. The four DNA stands, T1-T4 were mixed in stochiometric quantities in 10x tris-acetate-EDTA buffer (TAE) and DNase-free water to a working 1x buffer solution with the oligonucleotides. The solution was then subjected to a thermal annealing process, where it was heated at 95℃ for 5 minutes, 62℃ for 30 minutes, 50℃ for 30 minutes, 37℃ for 30 minutes, 25℃ for 30 minutes and allowed to cool at 4℃ for 30 minutes.

4.1.5 Preparation of blank DNA micelles

The nucleic acid micelles were prepared by slightly adapting a previously reported method (78). A stock solution of single-stranded DNA conjugated with cholesterol was diluted under acidic conditions and subjected to a thermal annealing process (**Figure 9)**. The final concentration of the sequence used to prepare the micelles was 20 μM.

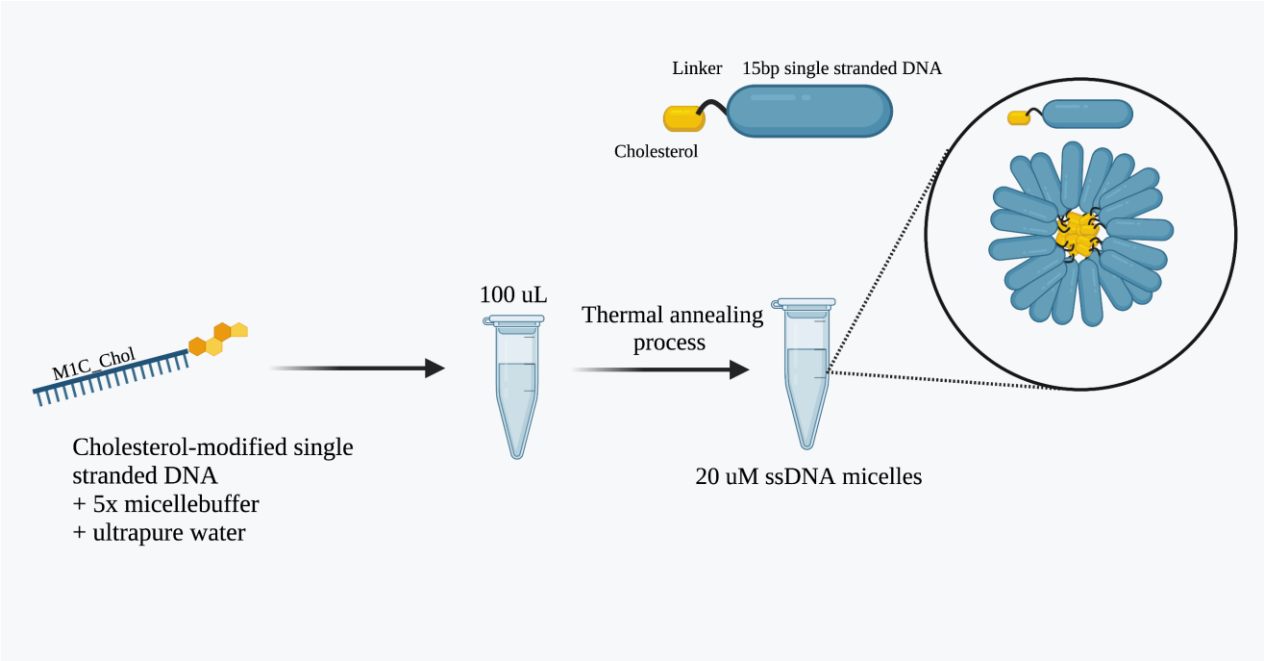

Figure 9*: Fabrication of unloaded ssDNA micelles.*

Briefly, the cholesterol conjugated ssDNA was mixed with a 5x micelle buffer (20 mM NaCl; 10mM $MgCl_2$; x sodium acetate; pH 4.5) and DNase free water to achieve a 1x working concentration buffer solution with the oligonucleotide. The solution was then heated at 37℃ for 30 minutes, and then from 37℃ to 29℃ decreasing 0.1℃ every 10 minutes, to prepare the self-assembled spherical micelles.

4.1.6 Preparation of polymyxin B loaded DNA micelles

A stock 1 mg/ml polymyxin B solution was prepared in water. From this stock solution, polymyxin B was added directly to ssDNA, 5x micelle buffer and water to prepare a 1x working concentration buffer solution with the oligonucleotide and polymyxin B (**Figure 10)**. In contrast to the ssDNA in itself (**Section 4.1.5**), this formulation did not need any thermal annealing process to form spherical micelles. A series of concentrations was tested for incorporation in the 20µM micelles and the effect on size, morphology and zeta potential was recorded for all concentrations.

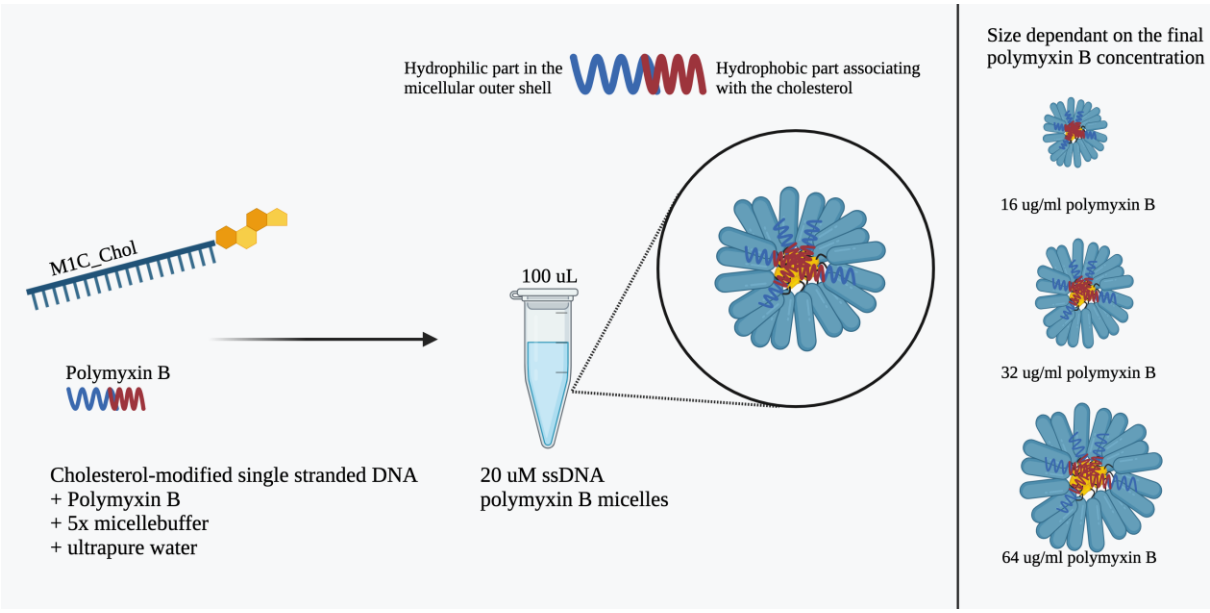

Figure 10: *Fabrication of the polymyxin B ssDNA micelles.*

4.2 Characterization

4.2.1 Hydrodynamic diameter, PDI and zeta potential

The dynamic light scattering (DLS) technique was used to measure the hydrodynamic diameter, polydispersity and surface potential of the formulations using a Malvern Zetasizer Nano-ZS (Malvern, Oxford, UK). For size measurements, a quartz low volume cuvette (ZEN2112, Malvern Panalytical) was filled with the nanoparticles in their native concentration. For zeta potential measurements of the same formulations, a high concentration zeta potential cell (ZEN1010, Malvern Panalytical) was filled with a 2x dilution of the formulations in filtered tap water. All measurements were made at a temperature of 25℃. Measurements was carried out

for two batches of the formulations and each reading was collected in triplicates. The result was reported as mean ± standard deviation (n=2)

4.2.2 Nanoparticle stability

The relative change in hydrodynamic diameter, polydispersity, and zeta potential of NNP, NNP^{Chi} and NMC was examined over a period of 14 days. The formulations were stored at 4℃ and measurements were made at day 0, day 1, day 7 and day 14. Results are reported as the relative change in hydrodynamic diameter, PDI and zeta potential. Measurements were carried out at a temperature of 25℃. Measurements were carried out for one batch of the formulations and each reading was collected in triplicates. The result is reported as mean ± standard deviation (n=1).

4.2.3 Morphology of DNA nanoparticles

The morphology on the nanoparticles was examined with the transmission electron microscope (TEM). Briefly, 50-100 x dilution of the samples was prepared in 1x distilled water. The grids used for the evaluations were first glow discharged for 20 s and the samples placed on the grid to adsorb. After 5-10 minutes, the grid was blotted dry and then stained with Uranyless solution for 20-40 s. After this time, the samples are washed with water and blotted dry. The grids are allowed to dry at room temperature for 20-30 minutes before imaging. Imaging was carried out using a transmission electron microscope model HT7800, Hitachi Ltd (Tokyo, Japan).

4.2.4 Gel electrophoresis

To assess the interaction between chitosan and the DNA nanostructures, agarose gel electrophoresis was used. A 2% agarose gel were prepared by dissolving 1g agarose in 50 ml tris-borate-EDTA buffer (TBE) under stirring and intermittent heating to assure all agarose was dissolved. To this solution, 5 µL SYBR SAFE nucleic acid gel stain was added, mixed, and the solution was cooled off in a cast with combs to make the gel. The gel was then mounted in the electrophoretic chamber, filled with TBE buffer and the samples were loaded (10 µL). Prior to loading, the samples were mixed with a 6x DNA loading dye, to make a 1x working dye

concentration with the samples. The tested samples were YSAF and chitosan 0.05%, 0.1%, 0.2% and 0.4% solutions added in equal volume and mixed. The gel was pictured using the gel imaging system Gel Doc XR+ with the accompanying analysis software (Bio-Rad Laboratories, CA, USA).

4.3 Polymyxin B entrapment efficiency (EE%)

The entrapment efficiency of polymyxin B in the micelles was evaluated using centrifugal filter units and UV spectroscopy. 100 µL of the PMB 64 µg/ml formulation was added to a centrifugal filter tube (molecular weight cutoff 3K) and the tube was centrifuged at 13 000 rpm for 10 minutes. After the centrifugation, the volumes from the donor and acceptor were collected and noted. The volume retrieved from the acceptor chamber was diluted 10x in water, and 50 µL of this dilution were added to a UV transparent 96-well plate. For the entrapped polymyxin B (donor chamber), a 10 x dilution was made in a new centrifugal filter tube with methanol to disrupt the formulation, which were then centrifuged for 3 minutes at 13 000 rpm. After centrifugation, 50 µL was added to a UV transparent 96-well plate and the absorbance was read at 210 nm, and the entrapment efficiency of polymyxin calculated based on absorbance values using a pre-obtained calibration curve.

4.4 Biofilm studies

4.4.1 Biofilm penetration experiments

Evaluation of each nanoparticle's ability to penetrate *P. aeruginosa* biofilms was done via imaging and quantitative methods. For all biofilm experiments, a colony of bacteria was taken from a fresh agar plate, added to 5 mL Mueller Hinton Broth (MHB) and incubated for 18-24 hours (37 °C, 100 rpm). The optical density (OD) of the culture was measured at 600 nm with a UV-spectrophotometer and adjusted to 0.07 (10^8 colony forming units (CFU)/mL) and was further 100x diluted (10^6 CFU/mL) in fresh MH media. Aliquots of 100 µL were added in duplicates to a transparent 96-well plate and incubated for 16 hours at 30°C. After incubation, the unattached planktonic bacteria were gently removed, and the formulations were added in 100 µL aliquots. Thereafter, the plate was set to incubate at 30°C for 2 hours. As a control, a

filtered solutions of the buffers used to fabricate the nanoparticles was used. After incubation the extent of penetration was investigated using the Quant-it PicoGreen assay method (**Section 4.4.1.1**), fluorescence spectroscopy or confocal imaging.

4.4.1.1 dsDNA quantification

The extent of nanoparticle penetration after treatment of the biofilms were assessed using Quant-iT PicoGreen dsDNA assay kit reagent for the DNA nanogel and tetrahedral formulations. The biofilms were formed as described in **Section 4.4.1**. An aqueous working solution of the reagent was prepared by making a 200-fold dilution of the concentrated DMSO solution in water. After biofilm treatment, the leftover media containing nanoparticles was collected from the treated wells, diluted 10 x in buffer (EB for nanogel samples, TAE for tetrahedral samples) and added in equal volumes to the diluted reagent solution. As a control, control biofilms that were treated with media containing the respective buffer solutions (EB for nanogel samples, TAE for tetrahedral samples) was also collected after 2h. To quantify the total DNA content in the DNA nanogels prior to treatment, the media collected from the control wells were used to dilute fresh nanoparticles. The controls were prepared in this manner to normalize the experiment for any DNA released from the biofilm during the experimental window. The solutions were then diluted 10 times and added in equal volume to the diluted reagent solution, as done for the sample-treated wells. Quadruplicate volumes of the samples were added to a costar black 96-well plate and the fluorescence intensity was measured using a plate reader.

4.4.1.2 Fluorescence spectroscopy

As an additional means to assess the nanoparticle penetration, the fluorescence intensity of the biofilms treated with different nanoparticles was determined. The biofilms were formed as described in 4.3.1, and the nanoparticles were prepared as fluorescently labelled formulations. After the 2-hour treatment, the medium in the wells were gently removed and then discarded. The biofilms were then directly measured for fluorescence intensity using a plate reader (Spark, Tecan) at an excitation and emission wavelength of 580 nm and 630 nm respectively.

4.4.1.3 Confocal laser scanning microscopy

Visualization of nanoparticle penetration in *P. aeruginosa* biofilm matrix was investigated using confocal laser scanning microscopy (CLSM). Biofilms were grown as previously described, in 8 well chambered slides for 16 hours (200 μL of the bacteria culture). After growing, the media was removed, discarded, and the biofilms were treated with 200 μL fluorescently labelled formulations for 2 hours. After the 2-hour treatment period, the formulations were carefully removed, and a working solution of SYTO9 green fluorescent nucleic acid stain was carefully added to the biofilm in 200 μL aliquots and set to incubate at room temperature for 20-30 minutes protected from light. After the incubation, the dye was carefully removed. Prior to imaging the treated biofilms were washed with sterile water to remove nanoparticles which were unbound/unpenetrated. Thereafter the penetrated nanoparticles were observed using CLSM (LSM 800, Zeiss).

4.4.2 Biofilm inhibition

To assess the biofilm´s mass after co incubation with nanoparticles, a crystal violet 0.1% v/v solution was prepared by diluting a 1% v/v stock solution. 100 μL aliquots were added to stain treated biofilms for 10 minutes. The staining solution was then gently removed from the wells and the biofilms washed with deionized water. The stain was then solubilized by adding 100 μL DMSO to each well, and then further diluted 4 times in separate wells with fresh DMSO before measuring absorbance at 595 nm using a microplate reader (Spark, Tecan). The control wells (untreated) were set to 100%, and treated wells were reported as relative amount to these controls.

4.5 Calorimetry-based biofilm assays

To assess NMC^{PMB} effect on mature biofilm and bacterial metabolism, biofilms were grown and analyzed using the calorimetric measuring system CalScreener (SymCel, Sweden). In brief, an overnight culture was grown, adjusted to OD 0.070 and diluted 100x as described in **Section 4.4.1**. Thereafter, 100 μL aliquots of the 1:100 dilution was made in sterile flat-bottom calWell inserts, which were subsequently fitted in the calPlate titanium vials and fitted with the cups. After assembly, the calPlate were carefully inserted into the Calscreener machine. After 18-

hour incubation, the calPlate with the biofilms was removed from the machine, the excess medium gently removed and 100 µL aliquots of the NMC, NMC^{PMB16}, NMC^{PMB32} and NMC^{PMB64} formulations was carefully added to the wells in duplicates. The calPlate was then reinserted into the machine, and the biofilms change in metabolic rate were monitored over 24 hours. For the analysis, the region of interest for max- and relative metabolic rate were set from time of addition to the time when the control wells reached baseline after addition. Three replicates were done for this experiment.

4.6 Cell culture

4.6.1 Seeding and treatment

The cell toxicity/biocompatibility of the formulations was investigated using immortalized human keratinocytes (HaCaT). The cells were cultured in cell culture flasks with Dulbecco´s Modified Eagle´s Medium (DMEM) high glucose (supplemented with 10% w/v fetal bovine serum (FBS) and 1% penicillin-streptomycin infused with serum). At approximately 80% confluency, the culture medium was discarded, and the keratinocytes attached to the flask were washed once with 10 ml phosphate-buffered saline (PBS). The PBS was discarded, and 4 ml Accutase® cell detachment solution was pipetted into the cell culture flask and set to incubate at 37℃ for 15 minutes. After the 15 minutes, the cells were agitated by vigorously mixing the solution with a pipette. The flask was then inspected under a microscope to ensure that the cells were properly detached. Thereafter, 10 ml fresh DMEM was added to the cell solution and thoroughly mixed with a pipette. The cell density of this solution was determined using a Scepter 2.0 handheld automated cell counter. The cells were then seeded with 200 µL in 96-well plates at a cell density of 6000 cells per well and set to incubate at 37℃ for 48 hours. The biocompatibility of the PMB formulations was investigated for PMB concentrations between 0.1 – 12.8 µg/ml serial dilution, with free PMB in the same concentrations serving as a positive control and DMEM as a negative control. For the drug-free formulations, a 5x dilution in DMEM was used, with the nanoparticles buffer serving as a positive control and DMEM as negative control. After the 48-hour incubation, the residual DMEM was removed and discarded gently. 100 µL of the samples were added in triplicate wells, and the plates were set to incubate at 37°C for another 48 hours. The cytotoxicity of the formulations was determined after the 48-

hour treatment incubation using the colorimetric 3-(4.5-dimethylthiazol-2-yl)-2.5-diphenyltetrazoliumbromide (MTT) assay.

4.6.2 MTT assay

As an indication for cell viability, the colorimetric MTT assay was used to determine the metabolic activity of the HaCaT cells after the 48-hour treatment incubation. In short, tetrazolium (MTT) powder was weighed and dissolved in ultrapure water to make a 7 mg/ml MTT solution in water. This stock was diluted in DMEM to make a 0.7 mg/ml MTT solution. The formulations were gently removed and discarded after the 48-hour incubation period. Thereafter, 200 μL of the 0.7 mg/ml MTT solution were added to each well and set to incubate at 37°C for 2 hours. After the 2 hours, the diluted MTT solution in DMEM was removed, and replaced with 100 μL DMSO in each well dissolve the formazan crystals produced. The cell viability was then determined by reading the absorbance at 570 nm using a microplate reader (Spark, Tecan).

5 RESULTS AND DISCUSSION

Rapid advances in DNA nanotechnology have highlighted the unique advantages of nucleic acid nanocarriers as ideal systems that can enhance targeting and reduce cytotoxicity of therapeutic cargos. Literature has illustrated their benefit as drug delivery platforms with improved cellular penetration into mammalian cells. Given the limited knowledge on applying DNA based nanocarriers in bacterial therapy, this study sought to tailor the physiochemical properties of DNA nanocarriers against bacterial biofilms, the highly treatment resistant and predominant state of bacteria in nature. Towards engineering DNA nanoparticles for this purpose, sequential modification to tune nanoparticle size, surface potential and amphiphilic character was performed. We fabricated hydrophilic and anionic DNA nanogels using three DNA nanostructures as our control system. Surface modification with chitosan to achieve cationic surface potential was performed. Given the significant increase in NP size following surface modification, tetrahedral NPs with a similar hydrodynamic diameter was prepared and compared (**Scheme 1)**.

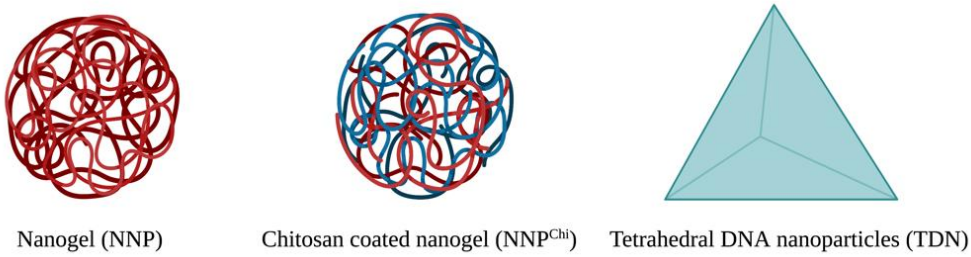

Scheme 1: Illustration of the unmodified DNA nanogel (NNP), chitosan coated nanogel (NNP^{Chi}) and DNA tetrahedron (TDN) formulations.

Finally, amphiphilic DNA sequences bearing cholesterol modification were designed and fabricated into micelles with anionic surface potential (**Scheme 2).** The impact of the abovementioned modifications was assessed on biofilm penetration to identify the optimal formulation for further studies. We hypothesized that enhancing the biofilm penetration of

DNA carriers through rational design could aid the development of a non-toxic multifunctional systems for antibiotic delivery with sustained drug delivery and antibiofilm effect.

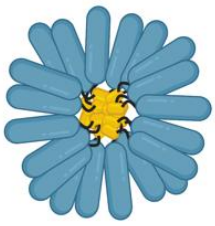

Cholesterol conjugated ssDNA micelles (NMC)

Scheme 2: Illustration of the DNA micelle nanoparticles (NMC).

5.1 Size and zeta potential of the blank nanoparticles

The physical attributes of nanomedicines have been demonstrated to significantly influence their biofilm penetration, drug efficacy, stability, and behavior *in vitro*/*in vivo* (91). For instance, the size of the nanocarrier is a key property in the clearance, biodistribution, toxicity and the nanoparticle-cell interactions (53). It is proposed that the diffusion coefficient of a nanoparticle decreases exponentially with the square radius of the particle, and that the ideal size of nanocarriers applied for antibiofilm applications does not exceed 300 nm. Nanoparticle size have also been determined to be an indicator on cell internalization, where smaller particles have increased cellular uptake. Additionally, the impact of the surface charge on nanoparticle biofilm penetration has been well established. Negatively charged nanoparticles will through electrostatic repulsion with the EPS components and bacterial membranes have limited interaction and hence result in the low efficacy of drug delivery systems in biofilms. Conversely, cationic nanoparticles have demonstrated great biofilm penetrating capability and increased cellular interaction. Furthermore, the surface charge of nanocarriers is an indicator on colloid stability, where NP-dispersions with zeta potential values of ± 30 mV are likely to be moderately stable formulations due to interparticle electrostatic repulsion (92). As such, the size and surface charge of the nanoparticle are two fundamental properties that dictate the performance of the delivery system.

DLS measurements were carried out to investigate the effect of surface coating and amphiphilic/hydrophilic character on size, polydispersity index and zeta potential.

a. Effect of surface coating

As shown in **Figure 6** and **7**, blank DNA nanogels were prepared comprising three nanostructures. The fabricated nanogel was further coated with chitosan (**Figure 8)** to ascertain the impact of surface coating on size, PDI and surface potential. As shown in **Figure 11A**, the unmodified nanogel formulation NNP had an average size of 52.5 ± 10.4 nm. Following surface coating, the NNP^{Chi} formulation showed a significant large increase in the size (297 ± 2.9 nm).

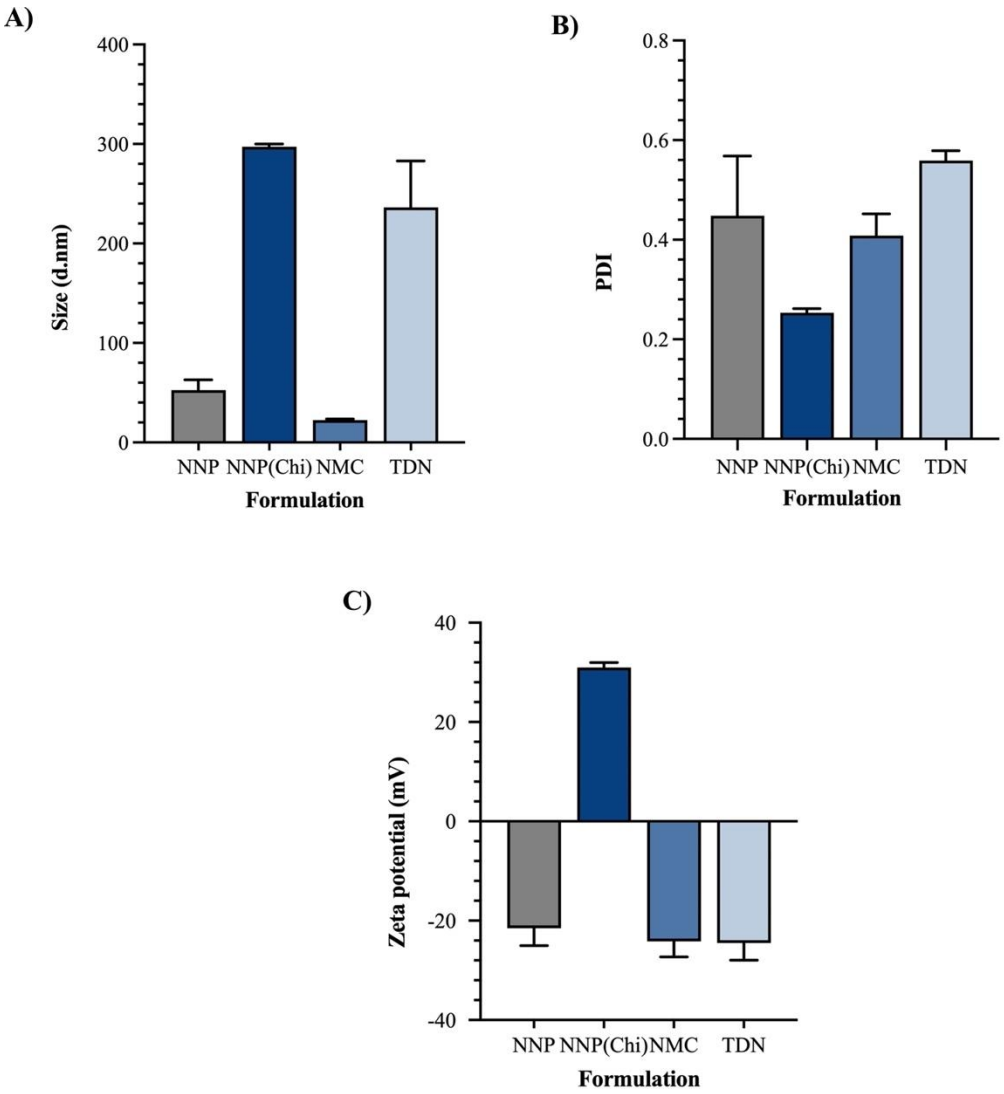

Figure 11: *DLS measurements of the blank nanoparticles, A) size, B) PDI and C) zeta potential. Values based on mean ± SD (n=2).*

This observed size of NNP^{Chi} is consistent with previously published papers which have investigated chitosan-DNA nanoparticles commonly being from 150-300 nm (93). We postulated that this effect was potentially due to non-covalent bonding of chitosan to DNA as a result of the electrostatic interaction between a cationic vector (chitosan) and a highly negatively charged molecule (DNA) (94). Specifically, this interaction is between the ionized phosphate groups of the ssDNA backbone and the protonated fraction of the chitosan.

To demonstrate the interaction between the nanostructures and chitosan, gel electrophoresis was performed to highlight the impact of chitosan coating on the migration pattern of DNA through an agarose gel. Because the migration pattern of DNA is directly dependent on the size and charge of DNA-complex, it was expected that increasing the concentration of chitosan would slow DNA migration or retard it to a different degree than the free nanostructure. As presented in **Figure 12**, we observed a single band for the nanostructure alone (YSAF, Lane 1). At a low concentration of 0.05% and 0.1% chitosan coating (Lane 2 and 3 respectively), slowed migration of the nanostructure was observed with some characteristic tailing/smearing of the bands.

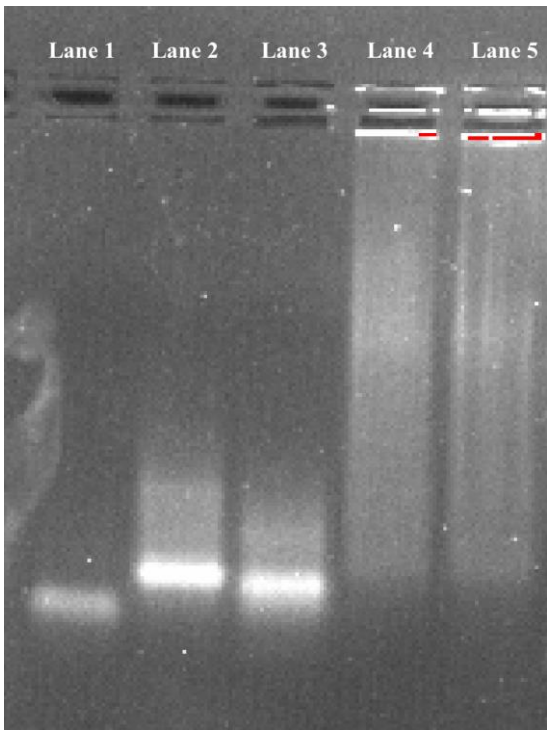

Figure 12: *Gel electrophoresis of hybridized Y-SAF (Lane 1), Y-SAF+0.05% chitosan (Lane 2), Y-SAF+0.1% chitosan (Lane 3), Y-SAF+0.2% chitosan (Lane 4) and Y-SAF+0.4% chitosan (Lane 5).*

This can be attributed to the increase in size of the nanostructure upon interacting with the polymer as well as change in the surface charge. At higher concentrations of 0.2% and 0.4% (Lane 4 and 5), band retardation was seen in the wells with significant smearing in the lane. This is attributed to the neutralization of DNA alongside formation of DNA-chitosan complexes with varying and increased molecular weights. Similar reports have been made, with the authors demonstrating the capability of cationic polymers to in part- or completely retard DNA (95, 96)

Following chitosan coating, a homogenous solution with a polydispersity index (PDI) of 0.25 ± 0.008 nm was seen for the NNP^{Chi} formulation compared to the observed multimodal size distribution of the NNP formulation (PDI value 0.45 ± 0.12 nm) **(Figure 11B**). We hypothesized that this could potentially be due to steric stabilization of the particles by the adsorbed chitosan. Indeed, the coating of nanoparticles with polymers is an established approach to increase colloid stability, and reports have been made that demonstrates the stabilizing properties of chitosan (97, 98). Finally, we investigated the impact of surface coating on the zeta potential of the NNP formulation. As illustrated in **Figure 11C**, zeta potential measurements showed a reversal from the highly anionic NNP (-21.5 ± 3.5 mV) to a positive surface charge of +30.9 ± 1.0 mV for NNP^{Chi}. At low concentrations of chitosan, there is a gradual neutralization of the highly negative charge of DNA as complexes are formed with chitosan. At higher concentrations, a rapid neutralization and a net increase to a positive value can be seen as the ratio of polymer increases. This observation has been demonstrated previously, where researchers found that chitosan coating could effectively turn negatively charged liposomes cationic (99)

To adequately compare the physical attributes of the abovementioned nanoparticles, we prepared another hydrophilic nanoparticle with comparable size to the NNP^{Chi} whilst exhibiting comparable surface potential to the NNP formulation. We reasoned that such a system will enable us to define the role of surface charge and size on biofilm penetration. While tetrahedral nanoparticles have been reported in literature with very small sizes, there is a consensus that modification of the buffer composition has a significant impact on size. A 2019 paper investigated the role of Mg2+ in the fabrication of tetrahedron DNA (100). In this work, the authors concluded that a suitable Mg2+ concentration is essential for the proper fabrication, and a too low concentration was associated with poor yield, aggregation, and existence of free DNA strands. We therefore prepared the tetrahedral nanoparticles in a tris-based buffer system that excluded magnesium. The resulting nanoparticle was also characterized for size, PDI and zeta potential. As shown in **Figure 11A**, the TDN formulation showed sizes of 236.3 ± 46 nm,

which is considerably larger than the average tetrahedron DNA framework (101). Nevertheless, the size was comparable to the chitosan formulation. The TDN formulation showed a multimodal distribution with PDI values of 0.55 ± 0.020 nm (**Figure 11B)**. The wide size distribution for the TDN formulation can be attributed to aggregation of the DNA strands due to the absence of Mg2+ in the formulation-buffer. Further evaluation of the surface potential showed a zeta potential of -24.5 ± 3.5 mV, a value also comparable to the NNP formulation.

b. Effect of sequence modification (amphiphilicity)

Towards understanding the role of amphiphilicity of DNA nanostructures on biofilm penetration, ssDNA sequences were designed bearing hydrophobic cholesterol modifications. The sequences self-assembled under specific buffer and thermal conditions to form spherical micelles. As shown in **Figure 11A**, the average size of the micellar formulations was 22.3 ± 1.3 nm. This was significantly smaller than the hydrophilic NNP, TDN and NNP^{Chi} and is potentially due to the mode of self-assembly, which is driven by the association of the cholesterol conjugations rather than sticky end ligation as for the other formulations.

The PDI of the NMC formulation was 0.36 ± 0.04 (**Figure 11B)**. Overall, the two modified formulations, NMC and NNP^{Chi} had a higher degree of particle uniformity in comparison to the unmodified particles (NNP and TDN) which had a more multimodal size distribution. A low PDI value is a key factor in identifying suitable formulations for *in vitro* and *in vivo* applications and gives an indicator of the particle's tendency to aggregate. Commonly for nanoparticles intended for drug delivery, PDI is regarded as a critical quality attribute, and a formulation is considered sufficiently monodisperse when the PDI value is < 0.3 (91). The observed zeta potential of the NMC formulation was -24.2 ± 3.15 mV (**Figure 11C)** which was similar to the NNP and the TDN formulations.

5.2 Nanoparticle stability

The preservation of the nanostructures properties as shape, composition, size and the surface property over time is vital for the quality of the nanocarrier. Aggregation during storage can alter the pre-defined and well-characterized physiochemical properties, which in turn has implications against adequate and reliable nanoparticle performance. Therefore, stability

studies were carried out for the NNP, NNP^{Chi} and NMC formulations over a period of 14 days at 4°C to evaluate the impact of surface or sequence modification on the possibility of significant aggregation over time. To achieve this, we compared the nanoparticles over the stipulated time by reporting on the relative change in hydrodynamic diameter and PDI from the day 0 measurements.

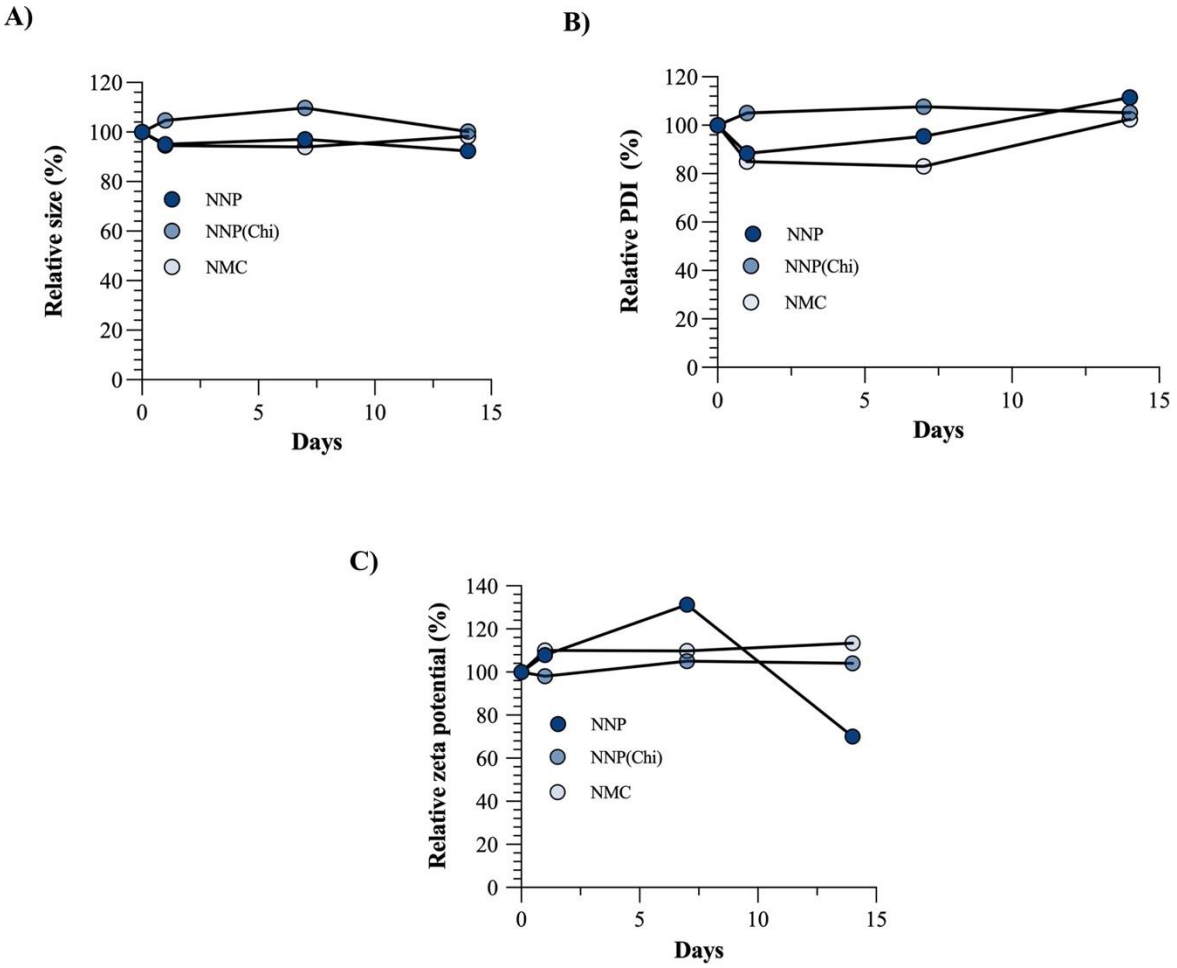

Figure 13: *Stability measurements of NNP, NNP and NMC – A) Size, B) PDI and C) zeta potential. Result is given as relative size in comparison with day 0 measurements.*

As demonstrated in **Figure 13A**, the formulations tested showed good overall stability in size over the 14-day period, with no relevant increase in the hydrodynamic diameter. After the 14-day period, the formulations had a relative change in size of -7%, +0.2% and +1.7% for the NNP NNP^{Chi} and NMC respectively. As for the polydispersity index, (**Figure 13B)** the blank DNA nanogel, NNP had the largest increase after 14 days (11.6%). The other formulations had a negligible increase of +5.1% and +2.5% for NNP^{Chi} and NMC respectively. These findings

indicate that significant alteration of the physicochemical properties of the modified formulations could not be observed demonstrating the absence of aggregation or agglomeration of these formulations under storage. In monitoring the change in zeta potential (**Figure 13C)**, we also observed the greatest change in zeta potential in the blank DNA nanogel with an increase in zeta potential of +32.2% on day 14. The other formulations exerted a slight drop in zeta potential with 4.8% and 13.4% for NNP^{Chi} and NMC respectively.

5.3 Morphology of the blank nanoparticles

The effect of nanoparticle morphology on its fate *in vivo* is thoroughly characterized. For instance, nanoparticles shape has been shown to directly influence the uptake into cells. For nanoparticles over 100 nm rod-shaped NPs seem to have the highest uptake, followed by spheres, cylinders, and then cubes (102). Oppositely, for smaller particles <100 nm, spherical micelles have a sizeable advantage in comparison with nanorods. Additionally, the morphology of nanoparticles has been found to be directly implicated in the efficacy of biofilm eradication, where certain shapes have shown significantly improve biofilm eradication than others (103). Bearing this in mind, the cholesterol-conjugated ssDNA formulation parameters were carefully selected to ensure spherical micelles were prepared that were of similar shape and size to the nanogels as reported in literature (90)

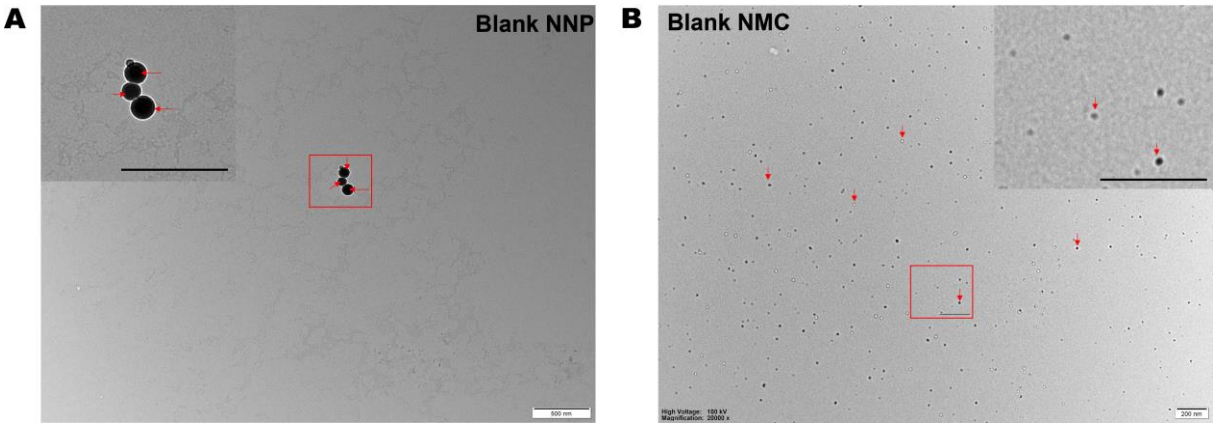

Figure 14: *Morphology of the A) blank NNP (scalebar: 500 nm) and B) blank NMC (scalebar: 200 nm) using TEM.*

TEM imaging was carried out to visualize the morphology of the nanoparticles and to correlate the results with the DLS findings. As can be seen in **Figure 14A**, successful formation of spherical shaped nanogels was seen with sizes that agree with the DLS findings. Similarly, we observed the formation of small and spherical micelles of approximately 20 nm using the cholesterol conjugated ssDNA which is analogous with what was determined via DLS (**Figure 14B)**. Considering the reported impact of buffer pH and salt content on the self-assembly of cholesterol modified DNA sequences, these results confirm that the chosen formulation parameters prevented aggregation and controlled the formation of spherical micelles (78). Typically, cholesterol-modified DNA nanostructures have been known to aggregate substantially by virtue of the hydrophobic tags, eliminating the structural control which makes DNA nanotechnology attractive (104). However, the findings herein confirms that the formulation of cholesterol modified ssDNA as micelles creates a highly stable system without the excessive aggregation commonly seen for cholesterol modified DNA formulations (**Figure 13B** and **Figure 14)**. We hypothesized that this is because the cholesterol tags associate to produce a core-shell micellar structure with the hydrophobic tag in the core, and DNA as an outer shell leading to interparticle electrostatic repulsion, limiting aggregation.

5.4 Biofilm penetration studies

One of the main obstacles for nanocarriers seeking to penetrate a bacterial biofilm is the complex network of biopolymers which protect the bacterial cells within, the EPS matrix. As such, antimicrobial drugs and peptides without the proper physiochemical properties may find little to no penetration and poor availability at the desired target site. Even so, by virtue of their cationic nature, several antimicrobial peptides such as polymyxin B have EPS-binding properties, hampering the antibacterial activity (105). To overcome this hurdle, enhanced drug delivery systems with desirable physiochemical properties that can penetrate deep into the biofilm can be utilized to increase the local drug concentration. Size, surface charge, hydrophilicity and shape are established indicators on how a nanocarrier will penetrate the biofilm matrix. As such, the binding and biofilm penetration of the developed nanocarriers were investigated to determine how these factors would affect the biofilm penetration of nucleic acid based nanocarriers.

First, we compared the biofilm penetration between nanoparticles that were formed using an in-house method that quantifies residual dsDNA following treatment. This assay was carried out for the formulations in which double stranded DNA is formed during the annealing process that could be quantified, i.e., that being the modified and unmodified nanogel formulations and the tetrahedral formulation. As shown in **Figure 15**, we evaluated the amount of penetrated nanocarrier in respect to the total amount applied to the biofilms.

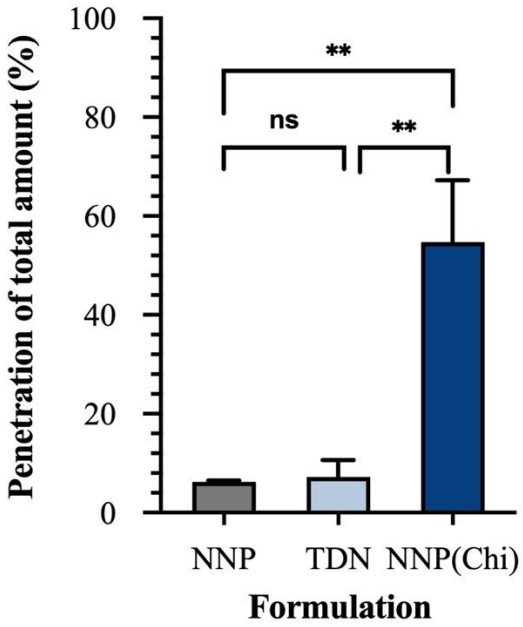

Figure 15: *In vitro biofilm penetration expressed by total amount penetrated in % measured by dsDNA quantification. Result based on mean ± SD (n=3).*

The pristine DNA formulations NNP and TDN showed negligible biofilm penetration after 2-hour incubation with 6.2 ± 0.2% and 7.2 ± 3.5% penetration respectively. We suggest that this low biofilm penetration is due to the combined hydrophilic and anionic nature of the nanocarriers. Anionic nanoparticles have been demonstrated to possess limited biofilm penetration, as result of electrostatic repulsion with EPS components (58). Although anionic nanoparticles penetrate less due to electrostatic repulsion with the anionic EPS, works have been published where the authors demonstrated some biofilm-penetrating capability of negatively charged liposomes (106). As such, we hypothesized that the hydrophilic nature of the nanogel and TDN formulation further reduced the biofilm penetration. The larger size and different morphology of the TDN formulations did not significantly alter the biofilm penetration in comparison with NNP (p=0.68). With 7.2 ± 3.5% penetration, we concluded that

the TDN formulation faces the same setbacks as NNP, and that the larger size of the formulation did not affect the biofilm penetration.

Next, the penetration of positively charged NNP^{Chi} formulation was evaluated. We observed a large increase in biofilm penetration than NNP. With 54.7 ± 12.5% penetration, NNP^{Chi} had a significantly increased biofilm penetration ($p=0.002$) in comparison with NNP. Since the TDN and NNP^{Chi} formulations are closely related in size (236 nm and 297 nm respectively), we postulated that this increased biofilm penetration was due to the positive charge surface chemistry of the formulation following surface modification, ruling out the effect of size on penetration. These findings agree with previously published works on nanoparticle-biofilm interactions, indicating that a positively charged DNA nanocarrier can effectively penetrate the biofilm of P. *aeruginosa* by virtue of its increased interaction with the biofilm components (58).

With the assay kit being very specific to dsDNA even in the presence of ssDNA, RNA and other free nucleotides, it was not feasible to get reliable measurements of the ssDNA micelles (NMC) using this assay, as several replicates showed very variable results **(Appendix Figure 2).** Therefore, we sought to determine the penetration of the micellar formulations via fluorescent measurements and confocal microscopy. **Figure 16** shows the relative fluorescence units (RFU) acquired by directly measuring the washed biofilms after 2-hour treatment. As seen in **Figure 16A**, the micellar formulation penetrated the biofilm, with an intensity of 40,181 compared to the untreated biofilm which had a relative fluorescence unit (RFU) of 582.

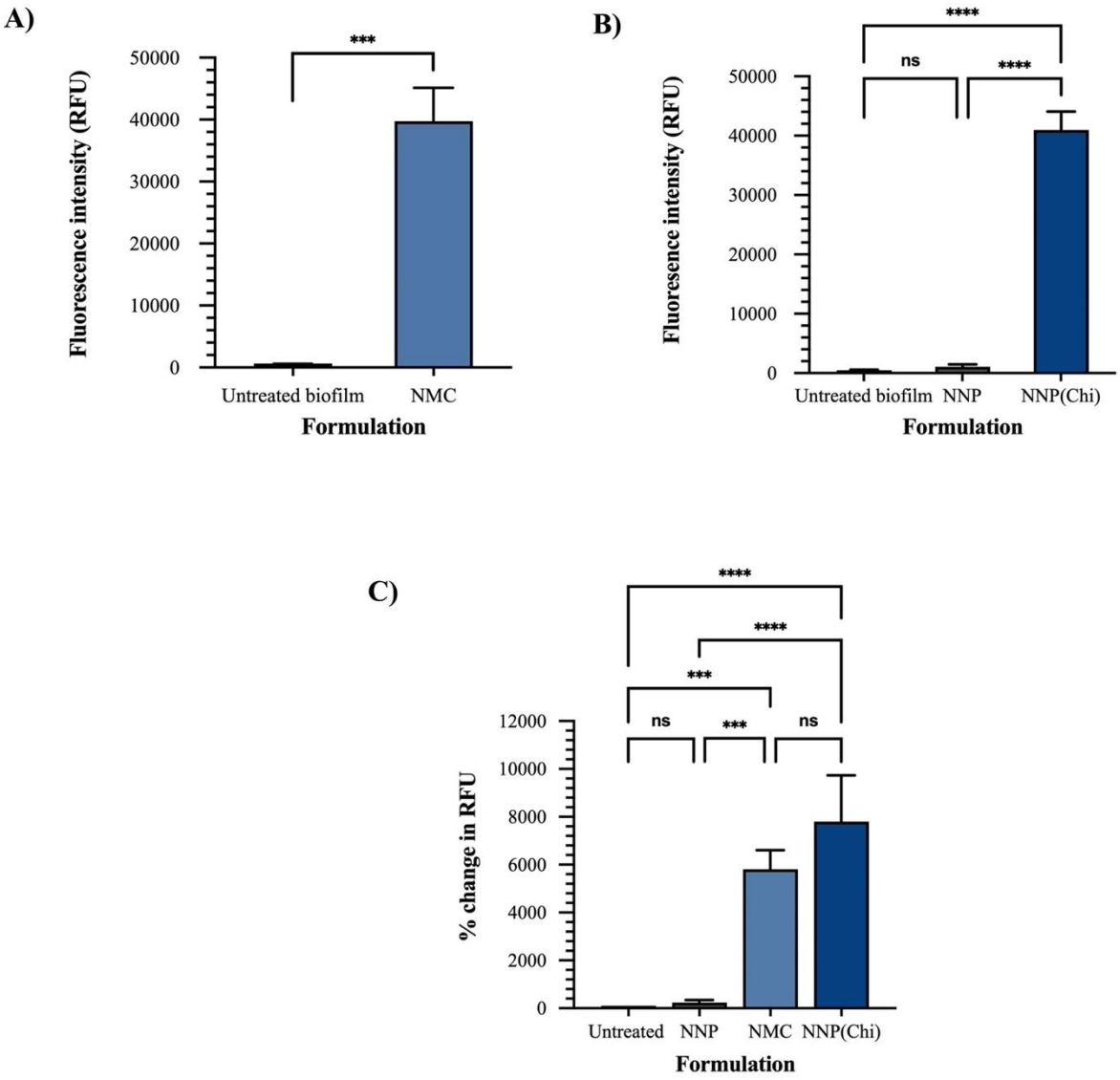

Figure 16: *In vitro biofilm penetration expressed in relative fluorescence units by directly measuring treated biofilms after treatment with A) NMC, B) NNP and NNP(Chi) and C) relative increase in RFU. Results based on mean ± SD (n=3).*

To correlate the dsDNA data and the observed penetration of the other formulations (**Figure 15)**, a fluorescent based assay was also carried out for the nanogel formulations, as seen in **Figure 16B**. These fluorescent based findings are analogous with what was determined via dsDNA quantification, with a much higher degree of penetration for the positively charged nanogel (NNP^{Chi} , 44338 RFU) in comparison with the unmodified nanogel (NNP, 781 RFU). Nevertheless, the observed fluorescence intensity of the biofilms after treatment with NMC was similar to $NNP^{Chi.}$ To compare the two modified formulations, the relative increase in RFU in

respect to untreated biofilms were plotted in **Figure 16C**. As shown, both the surface modification with chitosan and cholesterol conjugation drastically increased the RFU in comparison with untreated biofilm, indicating uptake into the biofilm matrix. Conversely, the unmodified NNP showed an insignificant 224 ± 110.7% ($p=0.99$) increase in comparison with the untreated biofilms, confirming the low biofilm penetration of the unmodified formulation. The modified formulations NMC and NNP^{Chi} showed an increase in RFU of 5811 ± 792% and 7789 ± 1936% respectively ($p=<0.001$). However, the findings indicated that no formulation penetrated the biofilm better than the other when compared ($p=0.15$). The findings suggest that both surface modification to endow the particle with cationic surface charge and the conjugation of cholesterol was equally effective in increasing the biofilm penetration of the carriers.

Given the similar penetration of the modified (NNP^{Chi} and NMC) and that of the unmodified (NNP vs TDN) nanoparticles, we visualized biofilm penetration assays with one representative formulation from each group. Specifically, the penetration of the NNP and NMC was compared via confocal microscopy. As seen in **Figure 17A,** after 2-hour exposure to NNP there was no observed fluorescence within the mature P. *aeruginosa* biofilms, with a more dominant green fluorescence from the bacteria. These results correlate the fluorescence measurement of the biofilms after treatment with the nanogels (**Figure 16B)**. In contrast, after 2-hour exposure to NMC there was a strong red fluorescence within the mature biofilms as seen in **Figure 17B**, the red from the formulation overshadows the bacterial stain, indicating a high degree of biofilm penetration.

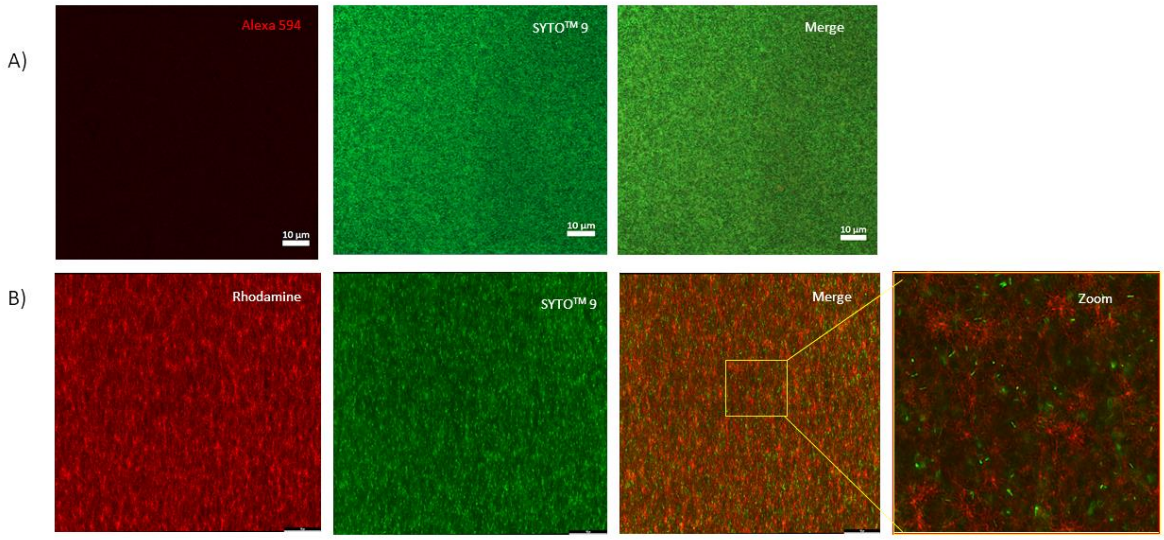

Figure 17: *In vitro biofilm binding and penetration assay in P.aeruginosa biofilms. CLSM 3D-images of A) NNP and B) NMC after 2 hour exposure.*

However, the zoomed image in **Figure 17B** showed no colocalization between the stained bacteria and the nanoparticles. This indicates that although the formulation penetrated the biofilm matrix, it did not penetrate or bind with the bacterial cell wall. We suspected that even though the small size and hydrophobicity increased the biofilm penetration, the negative surface charge made the nanoparticle-bacteria interaction slim. Whilst there is benefit in carriers that bind bacteria membranes to cause disruption, we envisioned that the micellar formulation owing to the great biofilm penetration could deliver high local doses of antibiotics or carry other biofilm-disruptive materials (such as gold nanoparticles or photosensitizers) (107-109). Additionally, given the small size, spherical morphology and high penetration of the NMC formulation, there is enormous potential to further develop this formulation for drug delivery applications against biofilm infections.

Therefore, the micellar DNA formulation was identified as the optimized platform and we further investigated the benefits of loading the antimicrobial peptide polymyxin B and its effect on P. *aeruginosa* biofilms.

5.5 Size and zeta potential of the optimized micelles – Polymyxin B loading

Polymyxin B is a lipopeptide which is commonly regarded as a last-resort antimicrobial agent against multi drug resistant (MDR) gram-negative bacteria, such as P. *aeruginosa* (110). Polymyxin B works by a detergent- like mechanism of action, where the polycationic peptide ring will bind to the outer membrane lipopolysaccharides (LPS) with a higher affinity than magnesium and calcium, destabilizing the LPS and subsequently disrupting the cell membrane. Further, the fatty acid chain will interact with the LPS, contributing to the insertion of polymyxin into the outer membrane, leading to permeability changes in the membranes. Affected membranes develop cracks, where a variety of intracellular molecules can leak, ultimately leading to cell death. Additionally, a second proposed mechanism is the inhibition of vital respiratory enzymes in the bacterial inner membrane which is crucial for respiration (111). As a consequence of the increasing rates of multidrug resistance in gram-negative bacteria, polymyxins have increasingly become the last viable therapeutic option for several MDR infections (112). Globally, the prevalence of P. *aeruginosa* resistance to polymyxin B is low (<5%), but some countries have seen an increase over the last years, implying that clinicians should be vigilant and call for new ways to effectively deliver PMB (113). The antimicrobial efficiency of cationic peptides is hampered as a result of interaction with EPS components, such as polyanionic eDNA through electrostatic interactions. This fact has been demonstrated for polymyxin b, where biofilm cells was more resistant to polymyxin B cells than planktonic (114). As such, incorporating the peptide in a carrier which can efficiently penetrate P. *aeruginosa* biofilms and protect polymyxin b from EPS interaction is attractive.

Given the amphiphilic nature of polymyxin B, we investigated whether formulation with the cholesterol modified sequence could drive self-assembly. To achieve this, PMB was mixed directly with cholesterol modified ssDNA under the same buffer conditions as the unloaded NMC formulation (**Figure 10).** We hypothesized that if PMB could effectively drive the self-assembly, the lengthy thermal annealing process of the unloaded NMC could be circumvented, shortening the fabrication process drastically.

Previous studies have demonstrated that the incorporation of cationic antibiotics into DNA carriers has an impact on nanoparticle size and zeta potential (90). Therefore, to investigate the role of drug loading on the size, PDI and zeta potential of the NMC formulations, three different final concentrations of polymyxin B was incorporated. A shown in figure **18A**, both the size

and PDI varies with increased concentration of PMB. For size, increased PMB concentration greatly increased the size of the nanoparticles. We observed no significant increase in size of the PMB micelles at 16 μg/mL of PMB. A small diameter of 19.74 ± 3.6 nm was seen, which is comparable with the unloaded NMC formulation (22.3 ± 1.3).

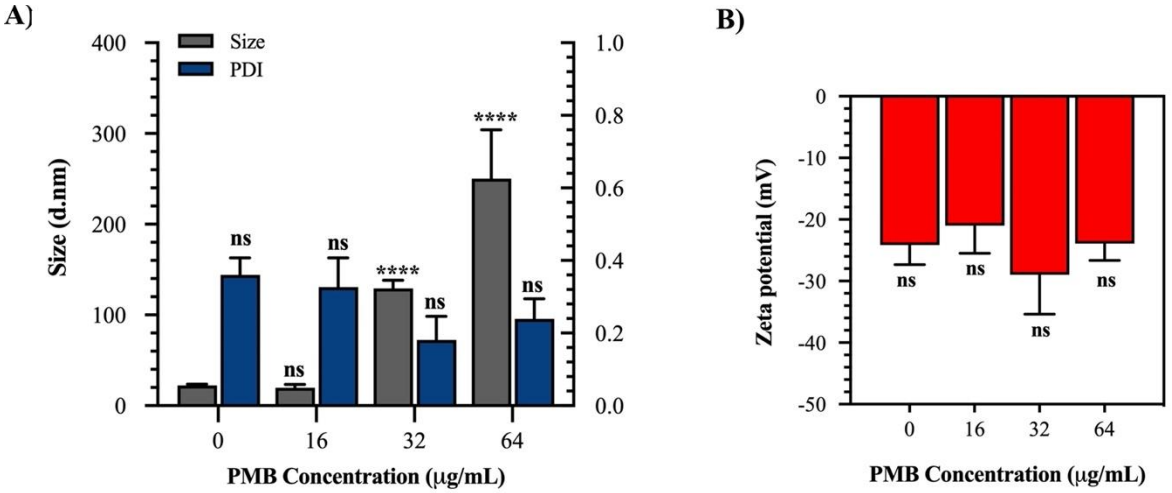

Figure 18: DLS *measurements of the PMB micelles with different concentrations of PMB loaded, A) Size and PDI and B) zeta potential. Values are based on mean ± SD (n=3).*

The similarity in size of the formulation indicates that amphiphilic nature of PMC was able to drive the self-assembly of the cholesterol micelles. We propose that this self-assembly is driven by the strong electrostatic interactions between the polycationic peptide ring of PMB and the negatively charged backbone of DNA, and the hydrophobic interaction between the long hydrophobic aliphatic chain of PMB and the cholesterol modification (**Scheme 3)**. Furthermore, PMB contains several carbonyl groups, indicating that they can form hydrogen bonds with the DNA phosphate backbone creating strong intermolecular interactions with the DNA (115)

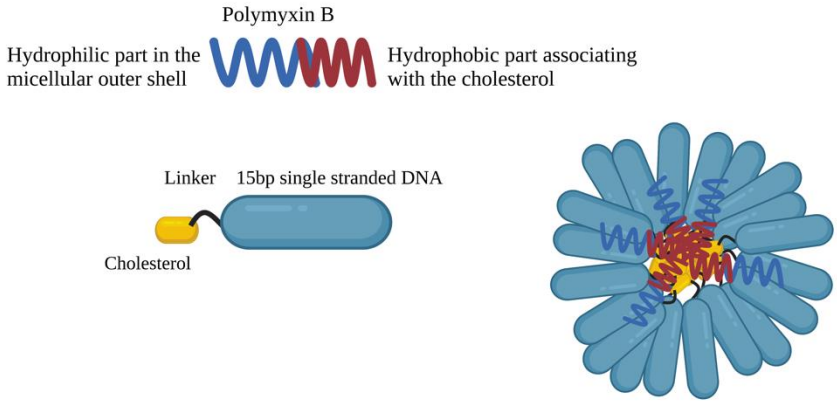

Scheme 3: *Illustration of the PMB loaded NMC with proposed method of incorporation.*

At 32 µg/mL of PMB, a significant increase to 129.5 ± 9.1 nm was observed. Similarly, when higher concentrations of PMB was loaded (64 µg/mL), there was a drastic increase in the size of the formulation, reaching an average diameter of 250.2 ± 53.4 nm. For the polydispersity index, increased PMB concentration promoted the formation of a monodisperse formulation. For instance, both micellar formulations loaded with 32 µg/mL or 64 µg/mL had PDI values below 0.3 (0.181 ± 0.081 and 0.239 ± 0.056 nm respectively). For drug delivery applications, a PDI of <0.3-0.2 and below is commonly considered to be desirable, and indicates a homogenous population of nanoparticles (91)

To investigate whether the incorporation of the drug was within the micelles as proposed or coated the carrier, we investigated the effect of zeta potential by comparing the surface charge of the blank micelles to that of the PMB loaded micelles. As shown in **Figure 18B**, increasing concentrations of PMB did not significantly alter the zeta potential, with the zeta potential recorded as -20.9 ± 4.5 mV, -28.9 ± 6.4 mV and -23.9 ± mV with increasing PMB concentrations, comparable with that of the unloaded NMC formulation having -24.2 ± 3.2 mV. These results demonstrate that PMB was trapped within the core of the micelles. Previous work on the incorporation of nanogels with cationic peptides have shown that in the case of surface coverage of the peptide, the negative charge of the carrier would be neutralized with a reversal to positive surface charge (90).

5.6 Morphology of the PMB loaded micelles

Thereafter, TEM imaging was performed to visualize the drug loaded micelles and to understand the effect of drug loading on the morphology of the micelles. We therefore performed TEM imaging for the micelles loaded with 32 µg/mL and 64 µg/mL. As shown in **Figure 19A**, the TEM image of the optimized formulation (32 µg/mL) illustrates the successful formation of spherical micelles, with similar appearance as the blank micelles. The formation of the micelles depicted in **Figure 19** did not require a thermal annealing process to form spherical nanoparticles.

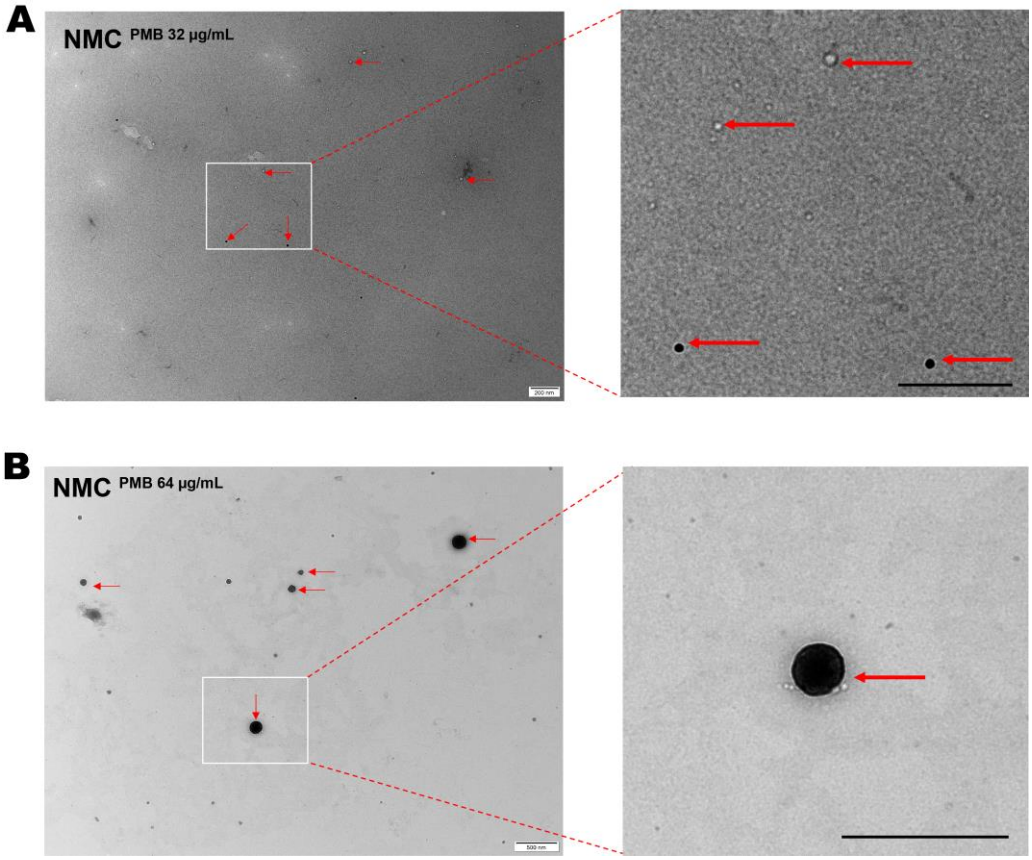

Figure 19: *Morphology of the optimized NMC formulations with A) 32 µg/mL and B) 64 µg/mL PMB loaded micelles using TEM (scalebar: 500 nm).*

This is a welcome change which greatly shortens the steps from thermal annealing of the oligonucleotide to finished nanoparticle, minimizing the critical steps in the fabrication of the particle. In fact, the micelles in **Figure 19** could be self-assembled within seconds, compared to the NMC requiring a 13 hour long annealing process.

As the NMC formulations were dependent on a long thermal annealing process, it is safe to say that the cholesterol-modified ssDNA will not associate to create spherical micelles without heating, and that the incorporation of polymyxin B is directly responsible for the spontaneous formation of the micelle. The observed smaller size of the micelles is likely attributed to the drying of the carriers prior to imaging with TEM. Nevertheless, upon increasing the concentration of PMB to 64 μg/mL, we observed even larger nanoparticles which correlates the increased size from lower concentrations of the drug. Additionally, the nanoparticles also displayed spherical appearance (**Figure 19B)**. These results indicate that although there was an increase in size with drug loading, the formulation did not lose its sphericity.

5.7 PMB entrapment efficiency (EE%) and biofilm inhibition studies

Among the physiochemical properties used to characterize a drug loaded nanocarrier, the entrapment efficiency (EE) is a crucial parameter which defines the percentage of the initial drug amount that is incorporated in the formulation (116). To determine this fraction, the nanocarrier-associated drug and free-bound drug is measured and evaluated in respect to the total quantity incorporated, commonly using centrifugation or dialysis. The efficiency of antimicrobial agents can be increased by encapsulation in a nanocarrier, and the efficiency in which this encapsulation takes place are desired to be high. Low encapsulation efficiency as a result of low drug-formulation affinity can result in undesired leakage and burst release of the cargo, negating the desired benefits of a drug delivery system. As shown in **Figure 20A**, we observed approximately 96.7 ± 1.1% entrapment efficiency of polymyxin B in the NMC nanocarrier. The entrapment efficiency of polymyxin B have been demonstrated to vary depending on formulation and zeta potential. For instance, Alipour and coworkers developed polymyxin liposomes using 1,2-dipalmitoyl-sn-glycero-3-phosphocholine (DPPC) and cholesterol, with an achieved entrapment efficiency of 32% (117). Chauhan and Bhatt developed polymyxin B niosomes with sorbitan monostearate and cholesterol to improve the poor intestinal permeability of polymyxin B. In this work, the niosomes varied in surface charge from -14 to -31 mV, and an EE% of 45-80% (118).

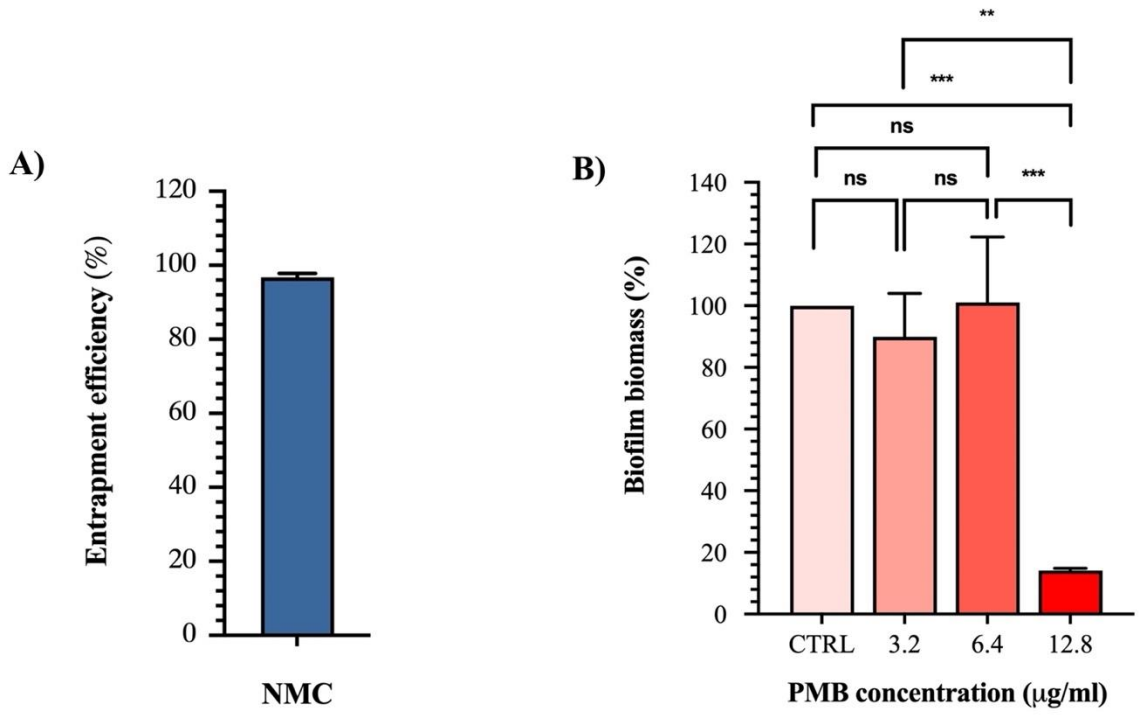

Figure 20: *A) Entrapment efficiency of NMC loaded with 64 μg/ml PMB and B) in vitro biofilm inhibition of PMB loaded NMC reported as relative biofilm mass to untreated biofilms*

The high entrapment efficiency can be attributed to the strong electrostatic interaction, hydrogen bonding and hydrophobic association between the cholesterol modified ssDNA and polymyxin B which was discussed in **Section 5.5**. The high affinity of polymyxin B to pristine DNA have been previously demonstrated, and the high EE% determined in this work agrees with previous findings (119). It would be advantageous to explore how this drug-formulation affinity affects the drug release in biologically relevant conditions.

Considering the observed high penetration of the micellar formulation blank NMC in P. *aeruginosa* biofilms, we hypothesized that the PMB loaded micelles could potentially sustain the release of the antimicrobial cargo in bacterial biofilms. Thus, we investigated the effect of the formulation in inhibiting biofilm formation and influence on mature biofilms. In the inhibition assay, we evaluated the effect of different PMB formulations (16, 32 and 64 μg/mL) diluted in the microbial medium at a final concentration of 3.2, 6.4 and 12.8 μg/mL. For the inhibition assay, CV staining was utilized, a well-established method that is known to be a good indicator of the amount of biomass (120)

As shown in **Figure 20B**, following co-incubation with the bacteria cells, the PMB loaded NMC showed a concentration dependent reduction in biomass. For the 3.2 μg/ml and 6.4 μg/ml group the measured biofilm mass was 89.91 ± 14.09% and 101 ± 21.26% respectively in comparison with the untreated group (100%). Nevertheless the 3.2 μg/ml and 6.4 μg/ml group did not significantly affect the biofilm formation under co-incubation for 16 hours (p=0.78 and 0.99 for 3.2 μg/ml and 6.4 μg/ml respectively). In contrast, the 12.8 μg/mL group showed a significantly reduced biofilm mass, with a measured biofilm mass of only 14.15 ± 0.74% (p=0.0002). These findings indicate that the incorporation of polymyxin B into the NMC created micelles which preserved the antimicrobial activity and released the cargo to significantly inhibit *P. aeruginosa* biofilms.

Calorimetry-based biofilm studies

To correlate the biofilm inhibition experiments and to further investigate the effect of the developed formulation on mature biofilms, a calorimetric based assay was carried out. Isothermal microcalorimetry (IMC) is a well acknowledged method used for measuring the energy released during metabolic processes in a biological system (121). Metabolically active bacteria will generate and release energy (heat flow) which is proportional to their growth rate in a culture system. Exposure of bacteria to antimicrobials will influence their metabolism and physiology, affecting the total energy released. IMC can measure the energy released at microwatt levels, making it a very sensitive tool to study the growth kinetics of bacteria, and have indeed been applied to susceptibility assays of biofilms to antimicrobials (122, 123).

We performed these experiments on biofilms treated with the three formulations added to the biofilms to achieve a final concentration of 12.8 μg/mL, 6.4 μg/mL and 3.2 μg/mL. Shown in Figure **21** is the impact of the different PMB concentrations on a variety of metabolic parameters. As can be seen in **Figure 21A** and **21B**, there was a significant change in the time to reach max metabolic activity (time to peak (TTP)) after treatment of the biofilms with the formulations.

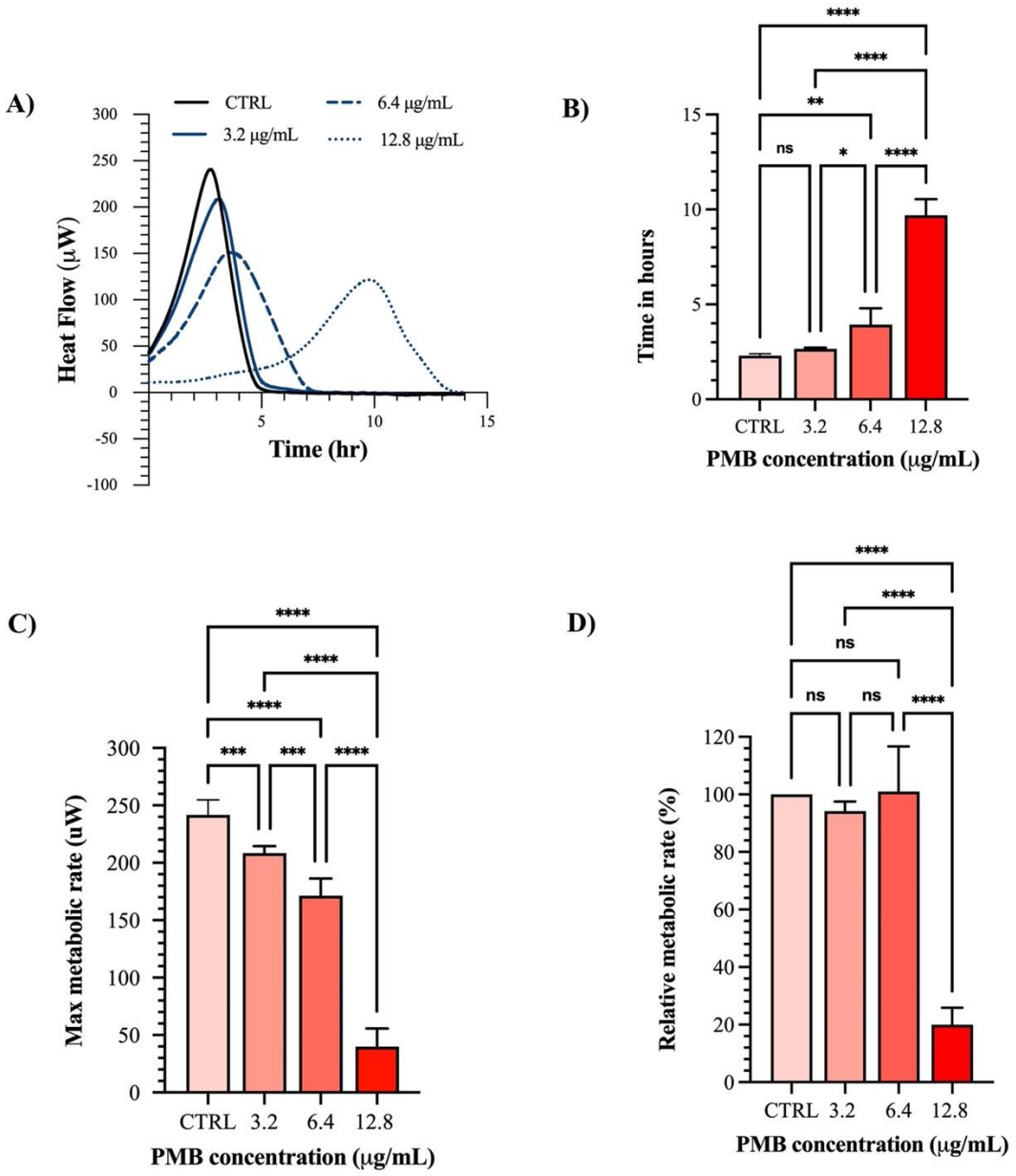

Figure 21: *Effect of PMB loaded NMC on selected metabolic parameters, A) and B) Time to peak metabolic activity, C) Max metabolic activity and D) relative metabolic activity. Results based on mean ± SD (n=3)*

A slight increase in TTP was seen after treatment with the 3.2 and 6.4 µg/mL groups. Specifically, the TTP was delayed 22 ± 3 minutes for the 3.2 µg/mL group and 98 ± 47 minutes for the 6.4 µg/mL group. A much more significant increase in TTP was seen after treatment with the 12.8 µg/mL group, where the treatment caused a 444 ± 50-minute delayed (7.4-hour) TTP. This delay can be attributed to an immediate release of PMB within the first few hours after treatment, followed by a sustained slower release.

To correlate the TTP data, metabolic rates within the same time frame (region of interest, ROI) for the formulations was plotted as max metabolic rate and relative metabolic rate. The ROI was chosen as directly after treatment (start) and 5 hours after treatment, when the control group reached baseline (**Figure 21A)** (end). As demonstrated in **Figure 21C**, there was a concentration dependent decrease in max metabolic activity for the formulations with 241 ± 12 uW for the drug-free control and 208 ± 6 uW, 171 ± 13 uW and 39 ± 14 uW for the PMB formulations with increasing drug concentration (3.2 μg/mL, 6.4 μg/mL and 12.8 μg/mL). All formulations showed a statistically significant reduction in max metabolic activity compared to the unloaded NMC. As can be seen in **Figure 21D**, the 12.8 μg/mL group had a vastly lower relative metabolic rate over the time period than the other formulations, with a 20 ± 5% relative metabolic rate to the drug-free control. For 3.2 μg/mL and 6.4 μg/mL groups, the relative metabolic rate was 94 ± 3% and 100 ± 14% respectively. This same concentration dependent decrease in relative metabolic rate within 0-5h after treatment is not seen for the lower concentrations because they did not significantly delay the time to peak in comparison with the control. The greatly reduced biofilm fitness demonstrated from these calorimetric data are analogous with the data presented in **Figure 20B** for biofilm inhibition indicating that the 12.8 μg/mL group effectively hindered biofilm formation and greatly reduced the metabolic activity in pre-formed, mature biofilms.

5.8 Cytotoxicity

The biocompatibility of a nanoparticle and/or active ingredients which is intended for use in humans is of great importance. Engineered nanoparticles may represent a toxicological challenge, and nanoparticles have been demonstrated to produce reactive oxygen species, induce protein misfolding, affect cell membrane permeability and directly damage cells (124). The size of nanoparticles makes them much more biologically active than micron-sized particles, allowing them to interact with cellular biochemical environments in a completely different manner (125). As such, the need for effective nanocarriers go together with the need for safe nanoparticles which exert their effect without significantly affecting the healthy cells. To assess the biocompatibility of the drug loaded formulations, the cell-viability tests were carried out using immortalized human keratinocytes. Epidermis, the outermost layer of the skin consists mostly of keratinocytes (>95%) and has been an essential tool in the study of skin-related diseases and infections (126). With the main application of the developed nanoparticles

being on skin- and soft tissue related infections, this cell line would provide the most relevant safety profile. The biocompatibility of free polymyxin B, polymyxin B, blank micelles, nanogel formulations and the tetrahedron formulation were evaluated *in vitro* in HaCaT cells.

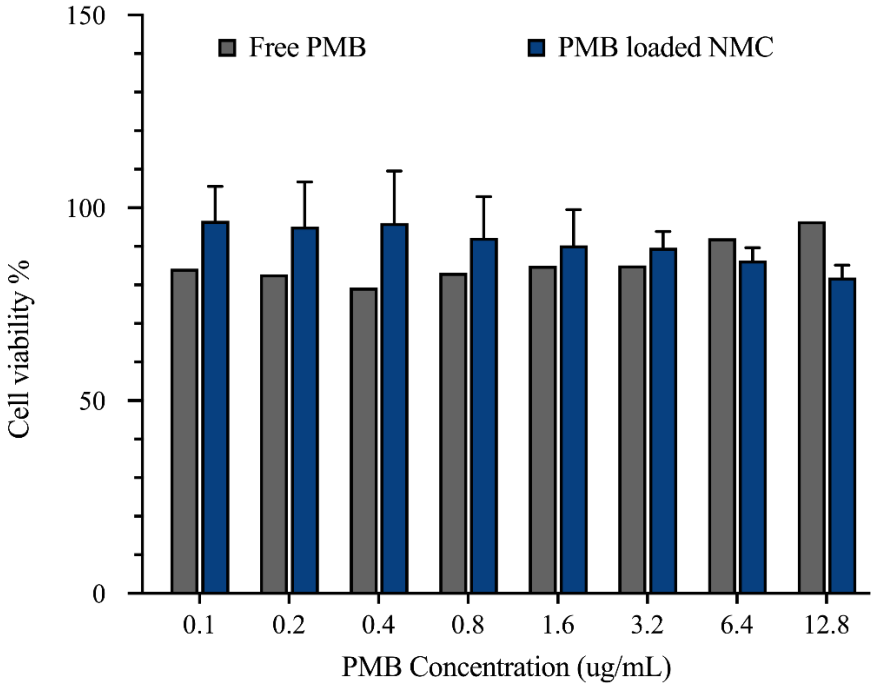

Figure 22: *Cytotoxicity of free polymyxin B and polymyxin B loaded NMC evaluated using HaCaT cells. Values based on mean +- SD (n=1 free polymyxin, n=2 polymyxin B micelles).*

Both free polymyxin B and the polymyxin B loaded micelles demonstrated overall low toxicity against the cell line for all concentrations (**Figure 22)**. For the highest concentration, 12.8 µg/mL both as formulation or free drug, exerted minimal toxicity with a cell viability of 82% ± 3.2% and 96.5 ± 2.1% respectively after the 48-hour incubation period in comparison to the buffer control. Standardized tests for cytotoxicity and thresholds are described in ISO 10993-5:2009, which is the international standard issued by the recognized authority on standards. This document states that reduction in cell viability by more than 30% is to be considered cytotoxic to the tested cell line. As such, none of the polymyxin B concentrations in formulation or free drug are considered to exert a cytotoxic effect. The goal for several nanoparticulate systems is to reduce toxic effects to healthy cells in comparison with free drug, by either securing a timely release of the cargo or a prolonged release. Against this cell line, the polymyxin B micelles did not increase cell viability significantly in comparison with free drug.

Despite not increasing the cell viability, the formulations of polymyxin B are still considered to be non-cytotoxic, demonstrating a high degree of compatibility with the HaCaT cells. Conversely, polymyxin B have been demonstrated to induce apoptotic cell death and DNA damage in other cell-lines, such as human alveolar epithelial cells and kidney epithelial (127). Moreover, this nephrotoxicity has been cited as a dose-limiting factor that can occur in up to 60% of patients, and is a major pharmacokinetic concern for the use of polymyxin B. As such, it would be beneficial to investigate how these micelles can improve this effect in other cell-lines.

The potential toxicity of a nanoparticle is heavily dependent on its physical properties like size, surface charge, shape and chemical composition (128). To exclude any potential toxicity from the blank NMC formulations, we performed MTT assay and compared the viability of HaCaT cells in the presence of the NMC and the other formulations. This was important as the developed nanoparticles varied greatly in surface charge, shape, size and buffer condition (pH, salt ions). The high biocompatibility of nucleic acid-based nanoparticles has been stated previously (90). Being a naturally occurring, endogenous biomolecule, it is not expected to exert toxic effects. As demonstrated in **Figure 23**, all the blank nanoparticles exceeded 90% viability. Specifically, we observed viabilities of 90% ± 16%, 99% ± 19%, 105% ± 15%, 111% ± 20% for NNP, NNP^{Chi}, NMC and TDN respectively.

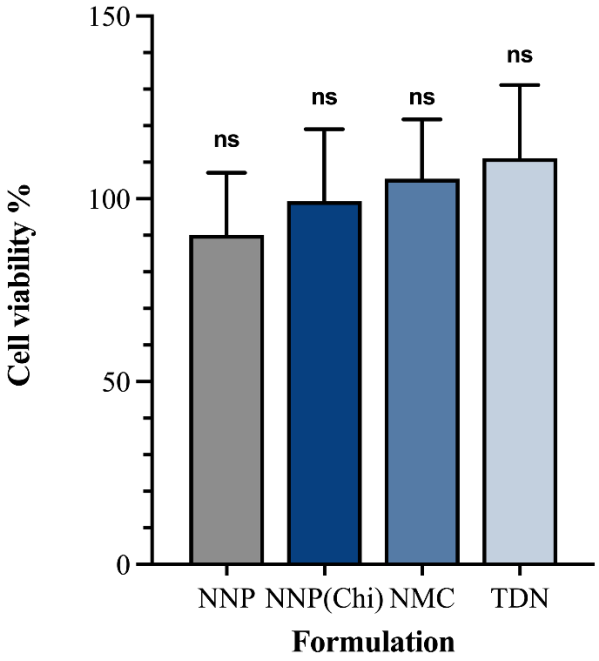

Figure 23: *Cytotoxicity of the blank nanoparticles. Values based on mean ± SD (n=3).*

This excellent biocompatibility further demonstrates the inherent advantage of nucleic acid-based particles in comparison with nanoparticles utilizing inorganic material and agrees with previous reports (90). Out of these nanoparticles, NNP^{Chi} has a positive surface chemistry. Cationic particles have been demonstrated to exert higher toxicity in comparison with negatively charged particles, owing to a higher degree of interaction with the negatively charged cell membrane. However, chitosan has been demonstrated to have an excellent biocompatibility with low cytotoxicity in concentrations which far precede that which the chitosan modified nanogels have (129). This fact is also evident in this data, as the chitosan coating did not significantly change the cell viability in comparison with the unmodified nanogel ($p=0.56$). Analyzing the mean percentage viability between all the groups showed no significant difference in the cell viability, indicating that the different modifications imposed on the carriers in this study did not alter the toxicity of the nanoparticles.

6 CONCLUSIONS

The main objective of this study was to determine the extent to which the physiochemical properties of nucleic acid-based carriers affected biofilm penetration. To achieve this, we sought to fabricate a series of nucleic acid-based nanoparticles with different properties via base-sequence modification and surface modifications to endow the nanocarriers with varying size, surface potential and hydrophobic modifications.

The series of nanoparticles NNP, $NNP^{Chi,}$ NMC and TDN were successfully fabricated. Characterization via DLS and TEM demonstrated that the nanoparticles had the desired physiochemical properties, and that NNP, NNP^{Chi} and NMC exhibited a good stability over 2 weeks with negligible changes in size, PDI and zeta potential. *In vitro* biofilm penetration of these formulations was assessed via CLSM, dsDNA quantification and fluorescent spectroscopy, which showed the ability of the modified formulations NMC and NNP^{Chi} to effectively penetrate *P. aeruginosa* biofilms converse to the poor penetration of the unmodified nanoparticles (NNP and TDN). These results demonstrate that surface modified nucleic acid-based particles (cationic) and cholesterol-conjugated ssDNA formulated as micelles can effectively penetrate *P. aeruginosa* biofilms. From these formulations, the micelles (NMC) were chosen as the optimal formulation for drug incorporation due to their relatively small size, ideal morphology, and high biofilm penetration. Moreover, in addressing the long fabrication process needed to formulate the NMC formulation, polymyxin B was shown to drive self-assembly within seconds further demonstrating the advantage of the NMC formulation as a delivery platform. Addition of polymyxin B to the cholesterol conjugated ssDNA produced spherical micelles, as confirmed via DLS and TEM imaging with a very strong affinity for the formulation (EE% of 96.7 ± 1.1%). Biofilm inhibition and the effect of the PMB loaded micelles on mature biofilms properties were assessed via crystal violet staining and calorimetric data, which showed the capacity of the formulations to significantly reduce biofilm formation and biofilm biomass in *P. aeruginosa* biofilms *in vitro*. All formulations were tested for toxicity against HaCaT cells, which demonstrated the already established cytocompatibility of pristine nucleic acid-based particles, and that the PMB loading into the micellar nanoparticles did not show significant toxicity.

In conclusion, tailoring the physiochemical properties of nucleic acid-based carriers allow them to overcome the poor biofilm penetration that is associated with the hydrophilic polyanionic nature of pristine DNA. We observed that, like other carriers, surface modification that endows the DNA nanoparticles with cationic surface chemistry and incorporation of hydrophobic moieties significantly increased the biofilm penetration in *P. aeruginosa* regardless of size. For the cholesterol modified DNA sequences, we propose that self-assembly of the spherical micelles could be driven in cooperation with amphiphilic peptide drugs, and that this achieves stable formulations with high drug entrapment. The resulting micelles showed good antibiofilm effect, high biocompatibility, and dose-dependent (antibiotic) size tunable properties. We propose that the NMC system holds tremendous potential for drug delivery in *P. aeruginosa* biofilms.

7 PERSPECTIVES

The findings from this study expands on the nascent field that is DNA nanomedicine in the treatment of biofilm infections. The modifications done in this work are promising strategies to significantly improve the biofilm penetration of DNA nanocarriers. Additionally, the findings open an avenue for the use of the DNA micelles previously reported by Zhang and coworkers (78) as an antibiofilm platform that holds tremendous potential when loaded with an antimicrobial peptide. Despite providing valuable insight in the use of DNA nanocarriers for antibiofilm applications in our work, it would be advantageous to explore a wider array of experimental conditions to better understand the performance of the materials. The following are some proposed future perspectives:

- Determination of size and surface charge characteristics could be explored in biologically relevant medium that would better mimic *in vivo* conditions to assess how a biomolecular corona will affect the physiochemical properties of the nanoparticles.

- Investigation of the antibacterial activity of the drug loaded formulation against other biofilm forming MDR bacteria, such as *S. aureus* or MRSA.

- Investigation of drug release from the PMB micelles in biologically relevant medium.

- Explore how the drug release profile could be altered, for instance via co-administration with DNase.

- Evaluation of cytotoxicity and biocompatibility of the drug-loaded micelles against other cell lines (for instance human alveolar epithelial cells and kidney epithelial cells).

- Evaluate the antibacterial efficacy of the drug-loaded micelles in an *ex vivo* skin explant or catheter model.

- Investigate whether the unmodified nanoparticles can be utilized in antifouling applications to prevent biofilm formation on surfaces.

8 REFERENCES

1. Gould IM, Bal AM. New antibiotic agents in the pipeline and how they can help overcome microbial resistance. Virulence. 2013;4(2):185-91.

2. Ventola CL. The antibiotic resistance crisis: part 1: causes and threats. P T. 2015;40(4):277-83.

3. Dadgostar P. Antimicrobial Resistance: Implications and Costs. Infect Drug Resist. 2019;12:3903-10.

4. Murray CJL, Ikuta KS, Sharara F, Swetschinski L, Robles Aguilar G, Gray A, et al. Global burden of bacterial antimicrobial resistance in 2019: a systematic analysis. The Lancet. 2022;399(10325):629-55.

5. Kolár M, Urbánek K, Látal T. Antibiotic selective pressure and development of bacterial resistance. Int J Antimicrob Agents. 2001;17(5):357-63.

6. Kapoor G, Saigal S, Elongavan A. Action and resistance mechanisms of antibiotics: A guide for clinicians. J Anaesthesiol Clin Pharmacol. 2017;33(3):300-5.

7. Munita JM, Arias CA. Mechanisms of Antibiotic Resistance. Microbiol Spectr. 2016;4(2):10.1128/microbiolspec.VMBF-0016-2015.

8. Abe K, Nomura N, Suzuki S. Biofilms: hot spots of horizontal gene transfer (HGT) in aquatic environments, with a focus on a new HGT mechanism. FEMS Microbiology Ecology. 2020;96(5).

9. Hoiby N, Flensborg EW, Beck B, Friis B, Jacobsen SV, Jacobsen L. Pseudomonas aeruginosa infection in cystic fibrosis. Diagnostic and prognostic significance of Pseudomonas aeruginosa precipitins determined by means of crossed immunoelectrophoresis. Scand J Respir Dis. 1977;58(2):65-79.

10. Jamal M, Ahmad W, Andleeb S, Jalil F, Imran M, Nawaz MA, et al. Bacterial biofilm and associated infections. J Chin Med Assoc. 2018;81(1):7-11.

11. Ciofu O, Moser C, Jensen PØ, Høiby N. Tolerance and resistance of microbial biofilms. Nature Reviews Microbiology. 2022.

12. Crouzet M, Le Senechal C, Brözel VS, Costaglioli P, Barthe C, Bonneu M, et al. Exploring early steps in biofilm formation: set-up of an experimental system for molecular studies. BMC Microbiol. 2014;14:253.

13. Rabin N, Zheng Y, Opoku-Temeng C, Du Y, Bonsu E, Sintim HO. Biofilm formation mechanisms and targets for developing antibiofilm agents. Future Med Chem. 2015;7(4):493-512.

14. Savage VJ, Chopra I, O'Neill AJ. Staphylococcus aureus biofilms promote horizontal transfer of antibiotic resistance. Antimicrob Agents Chemother. 2013;57(4):1968-70.
15. Borriello G, Werner E, Roe F, Kim AM, Ehrlich GD, Stewart PS. Oxygen limitation contributes to antibiotic tolerance of Pseudomonas aeruginosa in biofilms. Antimicrob Agents Chemother. 2004;48(7):2659-64.
16. Lewis K. Persister cells and the riddle of biofilm survival. Biochemistry (Mosc). 2005;70(2):267-74.
17. Wood TK, Knabel SJ, Kwan BW. Bacterial persister cell formation and dormancy. Appl Environ Microbiol. 2013;79(23):7116-21.
18. Reza A, Sutton JM, Rahman KM. Effectiveness of Efflux Pump Inhibitors as Biofilm Disruptors and Resistance Breakers in Gram-Negative (ESKAPEE) Bacteria. Antibiotics (Basel). 2019;8(4):229.
19. Zhang L, Mah T-F. Involvement of a novel efflux system in biofilm-specific resistance to antibiotics. J Bacteriol. 2008;190(13):4447-52.
20. Olsen I. Biofilm-specific antibiotic tolerance and resistance. European Journal of Clinical Microbiology & Infectious Diseases. 2015;34(5):877-86.
21. Flemming H-C, Neu TR, Wozniak DJ. The EPS matrix: the "house of biofilm cells". J Bacteriol. 2007;189(22):7945-7.
22. Flemming H-C, Wingender J. The biofilm matrix. Nature Reviews Microbiology. 2010;8(9):623-33.
23. Fong JNC, Yildiz FH. Biofilm Matrix Proteins. Microbiol Spectr. 2015;3(2).
24. Koo H, Xiao J, Klein MI, Jeon JG. Exopolysaccharides Produced by Streptococcus mutans Glucosyltransferases Modulate the Establishment of Microcolonies within Multispecies Biofilms. J Bacteriol. 2010;192(12):3024-32.
25. Nwodo UU, Green E, Okoh AI. Bacterial exopolysaccharides: functionality and prospects. International journal of molecular sciences. 2012;13(11):14002-15.
26. Karygianni L, Ren Z, Koo H, Thurnheer T. Biofilm Matrixome: Extracellular Components in Structured Microbial Communities. Trends in Microbiology. 2020;28(8):668-81.
27. Yamanaka T, Yamane K, Furukawa T, Matsumoto-Mashimo C, Sugimori C, Nambu T, et al. Comparison of the virulence of exopolysaccharide-producing Prevotella intermedia to exopolysaccharide non-producing periodontopathic organisms. BMC Infectious Diseases. 2011;11(1):228.

28. Eckhart L, Fischer H, Barken KB, Tolker-Nielsen T, Tschachler E. DNase1L2 suppresses biofilm formation by Pseudomonas aeruginosa and Staphylococcus aureus. Br J Dermatol. 2007;156(6):1342-5.
29. Sharma K, Pagedar Singh A. Antibiofilm Effect of DNase against Single and Mixed Species Biofilm. Foods. 2018;7(3):42.
30. Jakubovics NS, Shields RC, Rajarajan N, Burgess JG. Life after death: the critical role of extracellular DNA in microbial biofilms. Letters in Applied Microbiology. 2013;57(6):467-75.
31. Okshevsky M, Meyer RL. The role of extracellular DNA in the establishment, maintenance and perpetuation of bacterial biofilms. Critical Reviews in Microbiology. 2015;41(3):341-52.
32. Das T, Sharma Prashant K, Busscher Henk J, van der Mei Henny C, Krom Bastiaan P. Role of Extracellular DNA in Initial Bacterial Adhesion and Surface Aggregation. Appl Environ Microbiol. 2010;76(10):3405-8.
33. Kinch MS, Patridge E, Plummer M, Hoyer D. An analysis of FDA-approved drugs for infectious disease: antibacterial agents. Drug Discovery Today. 2014;19(9):1283-7.
34. Morel CM, Lindahl O, Harbarth S, de Kraker MEA, Edwards S, Hollis A. Industry incentives and antibiotic resistance: an introduction to the antibiotic susceptibility bonus. The Journal of Antibiotics. 2020;73(7):421-8.
35. Sercombe L, Veerati T, Moheimani F, Wu SY, Sood AK, Hua S. Advances and Challenges of Liposome Assisted Drug Delivery. Frontiers in Pharmacology. 2015;6(286).
36. Soares S, Sousa J, Pais A, Vitorino C. Nanomedicine: Principles, Properties, and Regulatory Issues. Frontiers in Chemistry. 2018;6(360).
37. Singh R, Lillard JW, Jr. Nanoparticle-based targeted drug delivery. Exp Mol Pathol. 2009;86(3):215-23.
38. Riehemann K, Schneider SW, Luger TA, Godin B, Ferrari M, Fuchs H. Nanomedicine—Challenge and Perspectives. Angewandte Chemie International Edition. 2009;48(5):872-97.
39. Pita R, Ehmann F, Papaluca M. Nanomedicines in the EU—Regulatory Overview. The AAPS Journal. 2016;18(6):1576-82.
40. Din FU, Aman W, Ullah I, Qureshi OS, Mustapha O, Shafique S, et al. Effective use of nanocarriers as drug delivery systems for the treatment of selected tumors. Int J Nanomedicine. 2017;12:7291-309.

41. Barenholz Y. Doxil® — The first FDA-approved nano-drug: Lessons learned. Journal of Controlled Release. 2012;160(2):117-34.
42. Wolfram J, Zhu M, Yang Y, Shen J, Gentile E, Paolino D, et al. Safety of Nanoparticles in Medicine. Curr Drug Targets. 2015;16(14):1671-81.
43. Greish K. Enhanced Permeability and Retention (EPR) Effect for Anticancer Nanomedicine Drug Targeting. In: Grobmyer SR, Moudgil BM, editors. Cancer Nanotechnology: Methods and Protocols. Totowa, NJ: Humana Press; 2010. p. 25-37.
44. Mitchell MJ, Billingsley MM, Haley RM, Wechsler ME, Peppas NA, Langer R. Engineering precision nanoparticles for drug delivery. Nature Reviews Drug Discovery. 2021;20(2):101-24.
45. Bao Z, Liu X, Liu Y, Liu H, Zhao K. Near-infrared light-responsive inorganic nanomaterials for photothermal therapy. Asian Journal of Pharmaceutical Sciences. 2016;11(3):349-64.
46. Qayyum S, Khan AU. Nanoparticles vs. biofilms: a battle against another paradigm of antibiotic resistance. MedChemComm. 2016;7(8):1479-98.
47. Wang C, Zhao W, Cao B, Wang Z, Zhou Q, Lu S, et al. Biofilm-Responsive Polymeric Nanoparticles with Self-Adaptive Deep Penetration for In Vivo Photothermal Treatment of Implant Infection. Chemistry of Materials. 2020;32(18):7725-38.
48. Ibelli T, Templeton S, Levi-Polyachenko N. Progress on utilizing hyperthermia for mitigating bacterial infections. International Journal of Hyperthermia. 2018;34(2):144-56.
49. Yuwen L, Sun Y, Tan G, Xiu W, Zhang Y, Weng L, et al. MoS2@polydopamine-Ag nanosheets with enhanced antibacterial activity for effective treatment of Staphylococcus aureus biofilms and wound infection. Nanoscale. 2018;10(35):16711-20.
50. Peng D, Liu G, He Y, Gao P, Gou S, Wu J, et al. Fabrication of a pH-responsive core–shell nanosystem with a low-temperature photothermal therapy effect for treating bacterial biofilm infection. Biomaterials Science. 2021.
51. Fulaz S, Vitale S, Quinn L, Casey E. Nanoparticle-Biofilm Interactions: The Role of the EPS Matrix. Trends Microbiol. 2019;27(11):915-26.
52. Dolai J, Mandal K, Jana NR. Nanoparticle Size Effects in Biomedical Applications. ACS Applied Nano Materials. 2021;4(7):6471-96.
53. Hoshyar N, Gray S, Han H, Bao G. The effect of nanoparticle size on in vivo pharmacokinetics and cellular interaction. Nanomedicine (Lond). 2016;11(6):673-92.
54. Peulen T-O, Wilkinson KJ. Diffusion of Nanoparticles in a Biofilm. Environmental Science & Technology. 2011;45(8):3367-73.

55. Nallathamby PD, Lee KJ, Desai T, Xu X-HN. Study of the multidrug membrane transporter of single living Pseudomonas aeruginosa cells using size-dependent plasmonic nanoparticle optical probes. Biochemistry. 2010;49(28):5942-53.
56. Meers P, Neville M, Malinin V, Scotto AW, Sardaryan G, Kurumunda R, et al. Biofilm penetration, triggered release and in vivo activity of inhaled liposomal amikacin in chronic Pseudomonas aeruginosa lung infections. J Antimicrob Chemother. 2008;61(4):859-68.
57. Fröhlich E. The role of surface charge in cellular uptake and cytotoxicity of medical nanoparticles. Int J Nanomedicine. 2012;7:5577-91.
58. Li X, Yeh Y-C, Giri K, Mout R, Landis RF, Prakash YS, et al. Control of nanoparticle penetration into biofilms through surface design. Chemical Communications. 2015;51(2):282-5.
59. Alhajlan M, Alhariri M, Omri A. Efficacy and Safety of Liposomal Clarithromycin and Its Effect on Pseudomonas aeruginosa Virulence Factors. Antimicrob Agents Chemother. 2013;57(6):2694-704.
60. Da Costa D, Exbrayat-Héritier C, Rambaud B, Megy S, Terreux R, Verrier B, et al. Surface charge modulation of rifampicin-loaded PLA nanoparticles to improve antibiotic delivery in Staphylococcus aureus biofilms. Journal of Nanobiotechnology. 2021;19(1):12.
61. Penders J, Stolzoff M, Hickey DJ, Andersson M, Webster TJ. Shape-dependent antibacterial effects of non-cytotoxic gold nanoparticles. Int J Nanomedicine. 2017;12:2457-68.
62. Aunkor MTH, Raihan T, Prodhan SH, Metselaar HSC, Malik SUF, Azad AK. Antibacterial activity of graphene oxide nanosheet against multidrug resistant superbugs isolated from infected patients. R Soc Open Sci. 2020;7(7):200640-.
63. Travers A, Muskhelishvili G. DNA structure and function. The FEBS Journal. 2015;282(12):2279-95.
64. Madhanagopal BR, Zhang S, Demirel E, Wady H, Chandrasekaran AR. DNA Nanocarriers: Programmed to Deliver. Trends in Biochemical Sciences. 2018;43(12):997-1013.
65. Seeman NC. Nucleic acid junctions and lattices. Journal of Theoretical Biology. 1982;99(2):237-47.
66. Seeman NC. DNA Nanotechnology at 40. Nano Lett. 2020;20(3):1477-8.
67. Zheng J, Birktoft JJ, Chen Y, Wang T, Sha R, Constantinou PE, et al. From molecular to macroscopic via the rational design of a self-assembled 3D DNA crystal. Nature. 2009;461(7260):74-7.

68. Obuobi S, Škalko-Basnet N. Nucleic Acid Hybrids as Advanced Antibacterial Nanocarriers. Pharmaceutics. 2020;12(7):643.
69. Wang W, Chen S, An B, Huang K, Bai T, Xu M, et al. Complex wireframe DNA nanostructures from simple building blocks. Nat Commun. 2019;10(1):1067.
70. Rothemund PWK. Folding DNA to create nanoscale shapes and patterns. Nature. 2006;440(7082):297-302.
71. Smith DM, Keller A. DNA Nanostructures in the Fight Against Infectious Diseases. Advanced NanoBiomed Research. 2021;1(3):2000049.
72. Qiu M, Singh A, Wang D, Qu J, Swihart M, Zhang H, et al. Biocompatible and biodegradable inorganic nanostructures for nanomedicine: Silicon and black phosphorus. Nano Today. 2019;25:135-55.
73. Sun W, Jiang T, Lu Y, Reiff M, Mo R, Gu Z. Cocoon-Like Self-Degradable DNA Nanoclew for Anticancer Drug Delivery. Journal of the American Chemical Society. 2014;136(42):14722-5.
74. Setyawati MI, Kutty RV, Tay CY, Yuan X, Xie J, Leong DT. Novel Theranostic DNA Nanoscaffolds for the Simultaneous Detection and Killing of Escherichia coli and Staphylococcus aureus. ACS Applied Materials & Interfaces. 2014;6(24):21822-31.
75. Hui L, Xu A, Liu H. DNA-Based Nanofabrication for Antifouling Applications. Langmuir. 2019;35(38):12543-9.
76. Tan LH, Xing H, Lu Y. DNA as a Powerful Tool for Morphology Control, Spatial Positioning, and Dynamic Assembly of Nanoparticles. Accounts of Chemical Research. 2014;47(6):1881-90.
77. Owens DE, Peppas NA. Opsonization, biodistribution, and pharmacokinetics of polymeric nanoparticles. International Journal of Pharmaceutics. 2006;307(1):93-102.
78. Zhang Y, Peng R, Xu F, Ke Y. Hierarchical Self-Assembly of Cholesterol-DNA Nanorods. Bioconjugate Chemistry. 2019;30(7):1845-9.
79. Li Z, Zhang Y, Fullhart P, Mirkin CA. Reversible and Chemically Programmable Micelle Assembly with DNA Block-Copolymer Amphiphiles. Nano Letters. 2004;4(6):1055-8.
80. Whitehouse WL, Noble JE, Ryadnov MG, Howorka S. Cholesterol Anchors Enable Efficient Binding and Intracellular Uptake of DNA Nanostructures. Bioconjugate Chemistry. 2019;30(7):1836-44.

81. Mao HQ, Roy K, Troung-Le VL, Janes KA, Lin KY, Wang Y, et al. Chitosan-DNA nanoparticles as gene carriers: synthesis, characterization and transfection efficiency. J Control Release. 2001;70(3):399-421.
82. Yan D, Li Y, Liu Y, Li N, Zhang X, Yan C. Antimicrobial Properties of Chitosan and Chitosan Derivatives in the Treatment of Enteric Infections. Molecules (Basel, Switzerland). 2021;26(23):7136.
83. Liu Y, Sun Y, Li S, Liu M, Qin X, Chen X, et al. Tetrahedral Framework Nucleic Acids Deliver Antimicrobial Peptides with Improved Effects and Less Susceptibility to Bacterial Degradation. Nano Letters. 2020;20(5):3602-10.
84. Mela I, Vallejo‐Ramirez PP, Makarchuk S, Christie G, Bailey D, Henderson RM, et al. DNA nanostructures for targeted antimicrobial delivery. Angewandte Chemie. 2020;132(31):12798-802.
85. Lu H, Wang J, Wang T, Zhong J, Bao Y, Hao H. Recent Progress on Nanostructures for Drug Delivery Applications. Journal of Nanomaterials. 2016;2016:5762431.
86. Obuobi S, Tay HK-L, Tram NDT, Selvarajan V, Khara JS, Wang Y, et al. Facile and efficient encapsulation of antimicrobial peptides via crosslinked DNA nanostructures and their application in wound therapy. Journal of Controlled Release. 2019;313:120-30.
87. Xu F, Xia Q, Wang P. Rationally Designed DNA Nanostructures for Drug Delivery. Frontiers in Chemistry. 2020;8.
88. Zhao Y, Sarkar A, Wang X. Peptide nucleic acid based tension sensor for cellular force imaging with strong DNase resistance. Biosens Bioelectron. 2020;150:111959-.
89. Perrault SD, Shih WM. Virus-Inspired Membrane Encapsulation of DNA Nanostructures To Achieve In Vivo Stability. ACS Nano. 2014;8(5):5132-40.
90. Obuobi S, Mayandi V, Nor NAM, Lee BJ, Lakshminarayanan R, Ee PLR. Nucleic acid peptide nanogels for the treatment of bacterial keratitis. Nanoscale. 2020;12(33):17411-25.
91. Danaei M, Dehghankhold M, Ataei S, Hasanzadeh Davarani F, Javanmard R, Dokhani A, et al. Impact of Particle Size and Polydispersity Index on the Clinical Applications of Lipidic Nanocarrier Systems. Pharmaceutics. 2018;10(2):57.
92. Bhattacharjee S. DLS and zeta potential – What they are and what they are not? Journal of Controlled Release. 2016;235:337-51.
93. Roy K, Mao HQ, Huang SK, Leong KW. Oral gene delivery with chitosan--DNA nanoparticles generates immunologic protection in a murine model of peanut allergy. Nat Med. 1999;5(4):387-91.

94. Bravo-Anaya LM, Soltero JFA, Rinaudo M. DNA/chitosan electrostatic complex. International Journal of Biological Macromolecules. 2016;88:345-53.
95. Rungsardthong U, Ehtezazi T, Bailey L, Armes SP, Garnett MC, Stolnik S. Effect of Polymer Ionization on the Interaction with DNA in Nonviral Gene Delivery Systems. Biomacromolecules. 2003;4(3):683-90.
96. Wu X-R, Zhang J, Zhang J-H, Xiao Y-P, He X, Liu Y-H, et al. Amino Acid-Linked Low Molecular Weight Polyethylenimine for Improved Gene Delivery and Biocompatibility. Molecules (Basel, Switzerland). 2020;25(4):975.
97. Schubert J, Chanana M. Coating Matters: Review on Colloidal Stability of Nanoparticles with Biocompatible Coatings in Biological Media, Living Cells and Organisms. Curr Med Chem. 2018;25(35):4553-86.
98. Aldawsari HM, Alhakamy NA, Padder R, Husain M, Md S. Preparation and Characterization of Chitosan Coated PLGA Nanoparticles of Resveratrol: Improved Stability, Antioxidant and Apoptotic Activities in H1299 Lung Cancer Cells. Coatings. 2020;10(5):439.
99. Bashiri S, Ghanbarzadeh B, Ayaseh A, Dehghannya J, Ehsani A. Preparation and characterization of chitosan-coated nanostructured lipid carriers (CH-NLC) containing cinnamon essential oil for enriching milk and anti-oxidant activity. LWT. 2020;119:108836.
100. Hu Y, Chen Z, Hou Z, Li M, Ma B, Luo X, et al. Influence of Magnesium Ions on the Preparation and Storage of DNA Tetrahedrons in Micromolar Ranges. Molecules. 2019;24(11).
101. Hu Y, Chen Z, Zhang H, Li M, Hou Z, Luo X, et al. Development of DNA tetrahedron-based drug delivery system. Drug Delivery. 2017;24(1):1295-301.
102. Albanese A, Tang PS, Chan WCW. The Effect of Nanoparticle Size, Shape, and Surface Chemistry on Biological Systems. Annual Review of Biomedical Engineering. 2012;14(1):1-16.
103. Tran HM, Tran H, Booth MA, Fox KE, Nguyen TH, Tran N, et al. Nanomaterials for Treating Bacterial Biofilms on Implantable Medical Devices. Nanomaterials (Basel, Switzerland). 2020;10(11):2253.
104. Ohmann A, Göpfrich K, Joshi H, Thompson RF, Sobota D, Ranson NA, et al. Controlling aggregation of cholesterol-modified DNA nanostructures. Nucleic acids research. 2019;47(21):11441-51.
105. Batoni G, Maisetta G, Esin S. Antimicrobial peptides and their interaction with biofilms of medically relevant bacteria. Biochimica et Biophysica Acta (BBA) - Biomembranes. 2016;1858(5):1044-60.

106. Dong D, Thomas N, Thierry B, Vreugde S, Prestidge CA, Wormald P-J. Distribution and Inhibition of Liposomes on Staphylococcus aureus and Pseudomonas aeruginosa Biofilm. PLOS ONE. 2015;10(6):e0131806.
107. Pinto RM, Soares FA, Reis S, Nunes C, Van Dijck P. Innovative Strategies Toward the Disassembly of the EPS Matrix in Bacterial Biofilms. Frontiers in Microbiology. 2020;11.
108. Ali SG, Ansari MA, Alzohairy MA, Alomary MN, AlYahya S, Jalal M, et al. Biogenic Gold Nanoparticles as Potent Antibacterial and Antibiofilm Nano-Antibiotics against Pseudomonas aeruginosa. Antibiotics (Basel). 2020;9(3):100.
109. Kim KR, Bang D, Ahn DR. Nano-formulation of a photosensitizer using a DNA tetrahedron and its potential for in vivo photodynamic therapy. Biomater Sci. 2016;4(4):605-9.
110. Zavascki AP, Goldani LZ, Li J, Nation RL. Polymyxin B for the treatment of multidrug-resistant pathogens: a critical review. Journal of Antimicrobial Chemotherapy. 2007;60(6):1206-15.
111. Deris ZZ, Akter J, Sivanesan S, Roberts KD, Thompson PE, Nation RL, et al. A secondary mode of action of polymyxins against Gram-negative bacteria involves the inhibition of NADH-quinone oxidoreductase activity. The Journal of Antibiotics. 2014;67(2):147-51.
112. Tam VH, Schilling AN, Vo G, Kabbara S, Kwa AL, Wiederhold NP, et al. Pharmacodynamics of polymyxin B against Pseudomonas aeruginosa. Antimicrob Agents Chemother. 2005;49(9):3624-30.
113. Chen X, Xu J, Zhu Q, Ren Y, Zhao L. Polymyxin B resistance rates in carbapenem-resistant Pseudomonas aeruginosa isolates and a comparison between Etest(®) and broth microdilution methods of antimicrobial susceptibility testing. Exp Ther Med. 2020;20(2):762-9.
114. Lima MR, Ferreira GF, Nunes Neto WR, Monteiro JdM, Santos ÁRC, Tavares PB, et al. Evaluation of the interaction between polymyxin B and Pseudomonas aeruginosa biofilm and planktonic cells: reactive oxygen species induction and zeta potential. BMC Microbiol. 2019;19(1):115.
115. Kong L, Liu Z, Hu X, Liu S. Interaction of polymyxin B with ds-DNA, and determination of DNA or polymyxin B via resonance Rayleigh scattering and resonance non-linear scattering spectra. Microchimica Acta. 2011;173(1):207-13.
116. Gaikwad VL, Choudhari PB, Bhatia NM, Bhatia MS. Chapter 2 - Characterization of pharmaceutical nanocarriers: in vitro and in vivo studies. In: Grumezescu AM, editor. Nanomaterials for Drug Delivery and Therapy: William Andrew Publishing; 2019. p. 33-58.

117. Alipour M, Halwani M, Omri A, Suntres ZE. Antimicrobial effectiveness of liposomal polymyxin B against resistant Gram-negative bacterial strains. Int J Pharm. 2008;355(1-2):293-8.
118. Chauhan MK, Bhatt N. Bioavailability Enhancement of Polymyxin B With Novel Drug Delivery: Development and Optimization Using Quality-by-Design Approach. J Pharm Sci. 2019;108(4):1521-8.
119. Yun B, Zhang T, Azad MAK, Wang J, Nowell CJ, Kalitsis P, et al. Polymyxin B causes DNA damage in HK-2 cells and mice. Arch Toxicol. 2018;92(7):2259-71.
120. Corte L, Casagrande Pierantoni D, Tascini C, Roscini L, Cardinali G. Biofilm Specific Activity: A Measure to Quantify Microbial Biofilm. Microorganisms. 2019;7(3).
121. Tellapragada C, Hasan B, Antonelli A, Maruri A, de Vogel C, Gijón D, et al. Isothermal microcalorimetry minimal inhibitory concentration testing in extensively drug resistant Gram-negative bacilli: a multicentre study. Clinical Microbiology and Infection. 2020;26(10):1413.e1-.e7.
122. Braissant O, Wirz D, Göpfert B, Daniels AU. Use of isothermal microcalorimetry to monitor microbial activities. FEMS Microbiology Letters. 2010;303(1):1-8.
123. Butini ME, Abbandonato G, Di Rienzo C, Trampuz A, Di Luca M. Isothermal Microcalorimetry Detects the Presence of Persister Cells in a Staphylococcus aureus Biofilm After Vancomycin Treatment. Frontiers in Microbiology. 2019;10.
124. Elsaesser A, Howard CV. Toxicology of nanoparticles. Advanced Drug Delivery Reviews. 2012;64(2):129-37.
125. de la Harpe KM, Kondiah PPD, Choonara YE, Marimuthu T, du Toit LC, Pillay V. The Hemocompatibility of Nanoparticles: A Review of Cell-Nanoparticle Interactions and Hemostasis. Cells. 2019;8(10):1209.
126. Choi M, Lee C. Immortalization of Primary Keratinocytes and Its Application to Skin Research. Biomol Ther (Seoul). 2015;23(5):391-9.
127. Ahmed MU, Velkov T, Lin Y-W, Yun B, Nowell CJ, Zhou F, et al. Potential Toxicity of Polymyxins in Human Lung Epithelial Cells. Antimicrob Agents Chemother. 2017;61(6):e02690-16.
128. Sukhanova A, Bozrova S, Sokolov P, Berestovoy M, Karaulov A, Nabiev I. Dependence of Nanoparticle Toxicity on Their Physical and Chemical Properties. Nanoscale Res Lett. 2018;13(1):44.
129. Rodrigues S, Dionísio M, López CR, Grenha A. Biocompatibility of Chitosan Carriers with Application in Drug Delivery. Journal of Functional Biomaterials. 2012;3(3).

130. Kohler TJ, Peter H, Fodelianakis S, Pramateftaki P, Styllas M, Tolosano M, et al. Patterns and Drivers of Extracellular Enzyme Activity in New Zealand Glacier-Fed Streams. Frontiers in Microbiology. 2020;11.
131. Forier K, Raemdonck K, De Smedt SC, Demeester J, Coenye T, Braeckmans K. Lipid and polymer nanoparticles for drug delivery to bacterial biofilms. Journal of Controlled Release. 2014;190:607-23.
132. Needham D, Anyarambhatla G, Kong G, Dewhirst MW. A New Temperature-sensitive Liposome for Use with Mild Hyperthermia: Characterization and Testing in a Human Tumor Xenograft Model. Cancer Research. 2000;60(5):1197.
133. Patra JK, Das G, Fraceto LF, Campos EVR, Rodriguez-Torres MdP, Acosta-Torres LS, et al. Nano based drug delivery systems: recent developments and future prospects. Journal of Nanobiotechnology. 2018;16(1):71.
134. Peng D, Liu G, He Y, Gao P, Gou S, Wu J, et al. Fabrication of a pH-responsive core–shell nanosystem with a low-temperature photothermal therapy effect for treating bacterial biofilm infection. Biomaterials Science. 2021.
135. Dwivedi S, Wahab R, Khan F, Mishra YK, Musarrat J, Al-Khedhairy AA. Reactive oxygen species mediated bacterial biofilm inhibition via zinc oxide nanoparticles and their statistical determination. PLoS One. 2014;9(11):e111289.
136. Xiu W, Shan J, Yang K, Xiao H, Yuwen L, Wang L. Recent development of nanomedicine for the treatment of bacterial biofilm infections. VIEW. 2021;2(1):20200065.

APPENDICIES

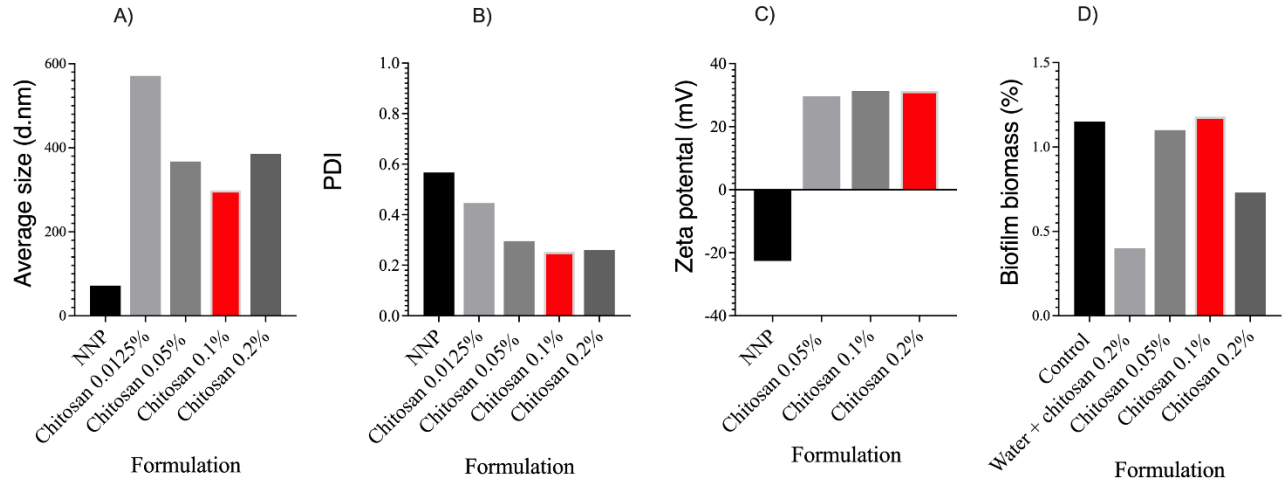

Appendix Figure 1: The effect on coating NNP with different concentrations on A) hydrodynamic size, B) PDI, C) zeta potential and D) P.*aeruginosa* biomass after 2 hour incubation. The concentration chosen for coating is highlighted in red .

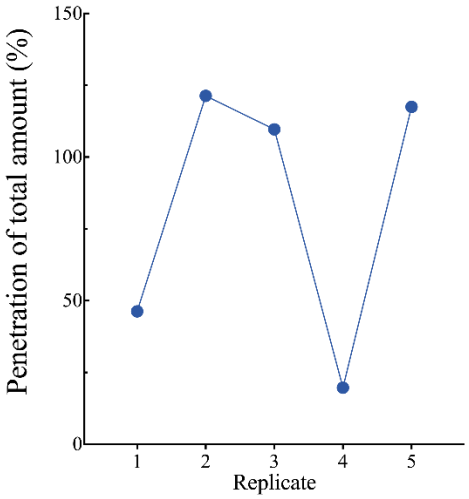

Appendix Figure 2: dsDNA quantification test runs for the NMC formulation.